UNIVERSIDADE DA BEIRA INTERIOR
Ciências da Saúde

Desenvolvimento de nanomateriais contendo IR780 para aplicação na terapia do cancro

Cátia Gomes Alves

Dissertação para obtenção do Grau de Mestre em
Ciências Biomédicas
(2º ciclo de estudos)

Orientador: Professor Doutor Ilídio Joaquim Sobreira Correia
Co-orientador: Mestre Duarte Miguel de Melo Diogo

Covilhã, junho de 2018

“Above all, don’t fear difficult moments. The best comes from them.”

Rita Levi-Montalcini

Para a Ikas ...

Agradecimentos

Em primeiro lugar quero agradecer ao Professor Ilídio Correia, por me ter dado a oportunidade de realizar a tese no seu grupo de investigação. Quero agradecer pelo seu apoio, por ter contribuído para que todo o trabalho se realizasse da melhor forma, pela sua ajuda e insistência para que eu fizesse cada vez mais e melhor.

Quero também dedicar um agradecimento ao meu co-orientador Duarte, por me ter ajudado a ser uma pessoa melhor, por toda a sua paciência, cuidado e insistência. Por me ter passado os melhores ensinamentos que alguma vez poderia encontrar! Obrigada por toda a dedicação, princípios e por acreditares sempre em mim.

A todo grupo de investigação, um obrigado por terem permitido que este ano fosse passado num ambiente de entreajuda e ao mesmo tempo cheio de bons momentos. Em especial à Beta, por toda a ajuda, apoio, experiência e gargalhadas partilhadas (és uma querida!), ao André por todos os ensinamentos e ajudas computacionais, à Sónia por todos os pedidos da "bomba"! Obrigada por me terem ajudado sempre que precisei! "Se fosse fácil, já estava feito".

À Rita, obrigada por teres sido uma parceira em tudo! À Sol, pelas boleias e viagens para "apanhar ar", à Sofs, por todas as risadas! A todas vocês, pelos momentos de stress e alegria partilhados!

Às minhas meninas, Chica, a minha irmã de faculdade (obrigada a ti, que vens desde o início dos inícios), Corina, por estares literalmente "sempre lá", Inêsita, por nunca me teres abandonado, Andreiiita "pisca", que este ano mostrou o quão "peste" e querida pode ser, Ritinha, que mesmo longe, tem sempre uma palavra de apoio para dar. A vocês, que me acompanharam ao longo destes 5 anos e que me aturaram e apoiaram mais que nunca neste último, quase 24 h por dia! Obrigada por todas as conversas, risadas e momentos que tornaram este ano mais leve e doce! Obrigada a vocês que fizeram da Covilhã "a minha casa".

Por fim quero agradecer à minha família, do fundo do coração. À minha mãe, aos meus pais, aos meus irmãos e à minha avozinha! Por me aturarem desde sempre e por me apoiarem em todas as minhas decisões! Sem vocês, nada disto teria sido possível... E finalmente, ao Ricardo por todo o apoio, toda a paciência e motivação diária, por estar sempre lá, apesar da distância! E por todo o amor, que nunca me deixou ir abaixo!

A todos, um muito obrigado por fazerem parte da minha vida! "Já deixaram um pouco de vocês" marcado em mim!

Resumo

O cancro da mama é uma das principais causas de morte nas mulheres em todo o mundo. Esta realidade deve-se em parte às limitações dos tratamentos usados na clínica, os quais apresentam baixa eficácia e induzem toxicidade não específica. Deste modo, existe uma necessidade crescente de desenvolver terapias inovadoras para o cancro.

Nos últimos anos, as fototerapias mediadas por nanomateriais têm demonstrado resultados promissores no tratamento do cancro. Este tipo de terapias tira proveito da capacidade das nanoestruturas para se acumularem preferencialmente na zona do tumor e posteriormente, ao serem irradiadas com luz com um comprimento de onda na zona do infravermelho próximo (NIR), produzirem um aumento de temperatura (terapia fototérmica) ou espécies reativas de oxigénio (terapia fotodinâmica), os quais podem induzir danos nas células cancerígenas. Para além disto, é também possível encapsular fármacos quimioterapêuticos no interior deste tipo de nanoestruturas, permitindo a sua utilização como agentes de quimio-fototerapia. Algumas nanoestruturas, após interação com a luz NIR, apresentam capacidade de emitir fluorescência, o que permite equacionar a sua utilização em imagiologia.

Na presente tese, desenvolveu-se um polímero anfifílico baseado em ácido hialurónico (HA) para formular micelas poliméricas concebidas para aplicação na quimio-fototerapia direcionada para o cancro da mama. Durante o processo de produção das micelas, a Doxorrubicina (agente quimioterapêutico) e o IR780 (agente responsivo à luz NIR com capacidade fototérmica, de fotossensibilização e de contaste de imagiologia) foram encapsulados no núcleo da micela. Os resultados obtidos revelaram que as micelas baseadas em HA (HPM) conseguem encapsular o IR780 (IR-HPM) e ainda permitem efetuar a co-encapsulação de IR780-Doxorrubicina (IR/DOX-HPM). Para além disto, verificou-se que a encapsulação do IR780 nas HPM aumenta a sua absorção (a 808 nm), em cerca de 2,2 vezes, comparativamente com o IR780 livre (não encapsulado), o que permite incrementar o potencial fototérmico das HPM. Por outro lado, a encapsulação do IR780 nos nanotransportadores também melhorou a sua citocompatibilidade. Nos ensaios de internalização *in vitro*, a fluorescência emitida pelas HPM foi utilizada para visualizar as células, tendo-se verificado que as HPM foram preferencialmente internalizadas pelas células do cancro da mama comparativamente com as células saudáveis. Estes resultados evidenciam o potencial destas nanoformulações para diagnóstico de cancro, bem como a sua capacidade de serem reconhecidas pelos recetores CD44 sobreexpressos na superfície das células cancerígenas. Nos ensaios de eficácia terapêutica, observou-se que as IR-HPM não causam efeitos citotóxicos consideráveis nas células do cancro da mama, enquanto a sua combinação com luz NIR induz uma redução da viabilidade celular. Por outro lado, a aplicação combinada das IR/DOX-HPM e luz NIR provocou uma diminuição ainda mais acentuada da viabilidade celular. Em suma, as HPM são nanoplataformas que apresentam propriedades

promissoras para a sua aplicação na quimio-fototerapia direcionada para o cancro da mama e imagiologia.

Palavras-chave

Cancro, Micelas Direcionadas, Quimioterapia, Terapia Combinatória, Terapia Fototérmica.

Resumo alargado

O cancro é atualmente uma das principais causas de morte em todo o mundo. Em particular, o cancro da mama surge como o mais comum e com maior taxa de mortalidade nas mulheres. Esta realidade deve-se em parte às limitações dos tratamentos usados na clínica (radioterapia e quimioterapia), os quais apresentam baixa eficácia e induzem toxicidade não específica. Deste modo, existe uma necessidade crescente de desenvolver terapias inovadoras para este tipo de cancro.

Nos últimos anos, as fototerapias têm demonstrado resultados promissores no tratamento do cancro. Neste tipo de terapia, usam-se agentes responsivos à luz que causam um aumento de temperatura (terapia fototérmica) e/ou produzem espécies reativas de oxigénio (terapia fotodinâmica), podendo assim induzir danos nas células cancerígenas. Os agentes responsivos à luz com um comprimento de onda no infravermelho próximo (NIR) são os mais utilizados, uma vez que a radiação neste intervalo (750-1000 nm) apresenta baixa interação com componentes biológicos (tais como água, melanina e hemoglobina) e elevada penetração nos tecidos.

O IR780 é um agente responsivo à luz NIR que tem potencial para ser aplicado nas terapias fototérmica e fotodinâmica. Esta molécula emite também fluorescência no NIR, pelo que pode ser usada como agente de contraste em aplicações de imagiologia. No entanto, o IR780 apresenta alguns problemas tais como baixa solubilidade em meio aquoso (hidrofobicidade) e citotoxicidade aguda. Estes problemas podem ser ultrapassados através da sua encapsulação em nanoestruturas, tais como micelas poliméricas. Para além disto, as micelas poliméricas conseguem encapsular fármacos quimioterapêuticos no seu interior, o que permite a sua utilização na quimio-fototerapia do cancro. No entanto, habitualmente as micelas não apresentam capacidade de direcionamento para as células cancerígenas, podendo assim exercer um efeito citotóxico tanto nas células cancerígenas como nas saudáveis que estão presentes no microambiente tumoral. Desta forma, a funcionalização das micelas com ligandos poderá melhorar o direcionamento destas para as células cancerígenas, contribuindo assim para atingir-se um efeito quimio-fototerapêutico mais seletivo.

No presente estudo, desenvolveu-se um polímero anfifílico baseado em ácido hialurónico (HA) para formular micelas poliméricas concebidas para aplicação na quimio-fototerapia direcionada do cancro da mama. Para tal, o HA foi usado como o componente hidrofílico do polímero anfifílico, devido à sua capacidade de se ligar aos recetores CD44, que estão sobreexpressos na membrana das células cancerígenas. Estes recetores encontram-se ainda num estado quiescente nas células normais (*i.e.*, não apresentam capacidade de ligar-se ao HA), confirmando assim o potencial destes como alvo de direcionamento. O HA desacetilado foi então ligado ao poli(anidrido maleico-*alt*-1-octadeceno) (PMAO) de forma a produzir o polímero

anfifílico que foi usado na produção das micelas. Posteriormente, a Doxorrubicina (agente quimioterapêutico) e o IR780 foram encapsulados no núcleo das micelas baseadas em HA (HPM), a fim de obter-se uma nanoformulação que possa ser utilizada em quimio-fototerapia.

Os resultados obtidos revelaram que as HPM, preparadas através do método de nanoprecipitação, apresentaram propriedades físico-químicas adequadas para a sua utilização na terapia do cancro. Verificou-se também que as HPM conseguem encapsular o IR780 (IR-HPM) e a combinação de IR780-Doxorrubicina (IR/DOX-HPM). Para além disto, constatou-se que a encapsulação do IR780 nas HPM aumenta a sua absorção no NIR (a 808 nm), em cerca de 2,2 vezes, comparativamente com o IR780 livre (não encapsulado), incrementando deste modo o potencial fototérmico das HPM. Por outro lado, o encapsulamento do IR780 também melhorou a sua citocompatibilidade. Nos ensaios de internalização *in vitro*, a fluorescência emitida pelas HPM foi utilizada para visualizar as células, tendo-se verificado que as HPM foram preferencialmente internalizadas pelas células do cancro da mama. Estes resultados evidenciam o potencial destas nanoformulações serem reconhecidas pelos recetores CD44, permitindo a sua utilização no diagnóstico e tratamento do cancro da mama. Nos ensaios de eficácia terapêutica, observou-se que as IR-HPM não causam efeitos citotóxicos consideráveis nas células do cancro da mama. No entanto, quando estes nanodispositivos são irradiados com luz NIR, ocorre uma redução da viabilidade celular em cerca de 40 %. Por outro lado, o efeito combinado das IR/DOX-HPM e luz NIR provocou uma diminuição da viabilidade celular em 80 %. Em suma, as HPM são nanoplataformas promissoras para aplicação em imagiologia e em quimio-fototerapia direcionada do cancro da mama.

Abstract

Breast cancer is a leading cause of death among women. This reality is in part owed to the sub-optimal efficacy and non-specific toxicity of the currently available treatments. In this way, there is an urge need to develop innovative therapies for breast cancer.

In the recent years, phototherapies mediated by nanomaterials have been showing promising results in cancer treatment. This type of therapy takes advantage from the ability of nanostructures to accumulate preferentially in the tumor zone. Afterwards, this site is irradiated with near infrared light (NIR) and nanomaterials upon interaction with NIR light, induce a temperature increase (photothermal therapy) or the formation of reactive oxygen species (photodynamic therapy), which can cause damage on cancer cells. Furthermore, nanostructures' core can also accommodate chemotherapeutic drugs, enabling their application in cancer chemo-phototherapy. Some nanostructures can also emit fluorescence upon exposure to NIR light, thus being promising for imaging applications.

Herein, a novel Hyaluronic acid (HA)-based amphiphilic polymer was synthesized and explored for the preparation of polymeric micelles aimed to be used for targeted breast cancer chemo-phototherapy. For such, Doxorubicin (chemotherapeutic agent, DOX) and IR780 (NIR-responsive photothermal agent, photosensitizer and imaging dye) were encapsulated in the micelles' core. The results revealed that HA-based micelles (HPM) were able to successfully encapsulate IR780 (IR-HPM) and the IR780-DOX combination (IR/DOX-HPM). Furthermore, the encapsulation of IR780 in HPM improved its absorption at 808 nm by about 2.2-fold, thereby enhancing its photothermal potential as well as its cytocompatibility. In the *in vitro* uptake studies, the fluorescence signals emitted by HPM were explored for cell imaging and the acquired data demonstrated that the nanostructures were preferentially internalized by breast cancer cells. These findings highlight the potential of these nanoformulations for CD44 targeting and cancer diagnosis. Moreover, IR-HPM alone did not induce any noticeable cytotoxicity to breast cancer cells. However, when this formulation was irradiated with NIR light a reduction on cancer cells' viability was obtained. The combined effect of IR/DOX-HPM and NIR light further decreased cancer cells' viability. Overall, based on the results obtained we can state that HPM are promising nanoplatforms for targeted chemo-phototherapy and imaging.

Keywords

Cancer, Chemotherapy, Combinatorial Therapy, Photothermal Therapy, Targeted Micelles.

List of Publications

Articles in peer reviewed international journals:

Alves, C.G.*, Lima-Sousa, R.*, de Melo-Diogo, D.*, Louro, R.O., Correia, I.J., 2018. IR780 based nanomaterials for cancer imaging and photothermal, photodynamic and combinatorial therapies. International Journal of Pharmaceutics 542, 164-175 (Doi: 10.1016/j.ijpharm.2018.03.020).

Alves, C.G., de Melo-Diogo, D., Lima-Sousa, R., Costa, E.C., Correia, I.J., Hyaluronic acid functionalized micelles loaded with IR780 and DOX for targeted cancer chemo-photothermal therapy. *Under review*.

Lima-Sousa, R., de Melo-Diogo, D., Alves, C.G., Costa, E.C., Louro, R.O., Correia, I.J., Functionalized green reduced graphene oxide for targeted cancer photothermal therapy. *Under review*.

de Melo-Diogo, D., Costa, E.C., Alves, C.G., Lima-Sousa, R., Louro, R.O., Correia, I.J., POxylated Graphene Oxide nanomaterials for combination chemo-phototherapy of breast cancer cells. *Under review*.

de Melo-Diogo, D., Lima-Sousa, R., Alves, C.G., Costa, E.C., Louro, R.O., Correia, I.J., Functionalization of graphene family nanomaterials for application in cancer therapy. *Submitted for publication*.

***** These authors contributed equally to this article.

Oral presentations in scientific conferences:

de Melo-Diogo, D., Pais-Silva, C., Costa, E.C., Alves, C.G., Lima-Sousa, R., Louro, R.O., Correia, I.J., Near infrared light responsive nanomaterials for cancer therapy, XVI Portuguese Conference on Fracture, TRYP Dona Maria, 23rd to 24th of April of 2018, Covilhã, Portugal.

de Melo-Diogo, D., Pais-Silva, C., Costa, E.C., Alves, C.G., Lima-Sousa, R., Louro, R.O., Correia, I.J., Near infrared light responsive nanomaterials for cancer therapy, VI Jornadas de Bioengenharia, Universidade da Beira Interior, 2nd to 3rd of May of 2018, Covilhã, Portugal.

Index

List of Figures

List of Tables

Abbreviation List

ANOVA	Analysis of Variance
Ce6	Chlorin e6
CLSM	Confocal Laser Scanning Microscopy
cRGD	Cyclic Arg-Gly-Asp
dHA	Deacetylated Hyaluronic Acid
DLS	Dynamic Light Scattering
DMEM-F12	Dulbecco's Modified Eagle's Medium-F12
DMSO	Dimethyl Sulfoxide
DOX	Doxorubicin
ECM	Extracellular matrix
EDC	1-Ethyl-3-(3-dimethylaminopropyl)carbodiimide
EE	Encapsulation Efficiency
EGFR	Epidermal Growth Factor Receptor
EPR	Enhanced Permeability and Retention
FBS	Fetal Bovine Serum
FDA	Food and Drug Administration
FTIR	Fourier Transform Infrared Spectroscopy
HA	Hyaluronic Acid
HA-*g*-PMAO	HA grafted PMAO
HPM	HA-based Polymeric Micelles
HSA	Human Serum Albumin
IC_{50}	Half Maximal Inhibitory Concentration
ICG	Indocyanine Green
IR/DOX-HPM	IR780-DOX loaded HPM
IR-HPM	IR780 loaded HPM
LC	Loading Content
MCF-7	Michigan Cancer Foundation-7
NHDF	Normal Human Dermal Fibroblasts
NHS	*N*-Hydroxysuccinimide
NIR	Near Infrared
ns	Non-significant
$^1O_2$	Singlet Oxygen
OATP's	Organic-Anion-Transporting Polypeptides
oPMAO	Hydrolysed PMAO
PBS	Phosphate Buffered Saline
PDI	Polydispersity Index

PDT	Photodynamic Therapy
PEG	Poly(ethylene glycol)
PFH	Perfluorohexane
PLGA	Poly(lactic-*co*-glycolic acid)
PMAO	Poly(maleic anhydride-*alt*-1-octadecene)
PPy	Polypyrrole
PTT	Photothermal Therapy
RES	Reticuloendothelial System
ROS	Reactive Oxygen Species
S.D.	Standard Deviation
TEM	Transmission Electron Microscopy
TOS	D-α-tocopheryl succinate
TPGS	D-α-tocopheryl polyethylene glycol succinate

Chapter 1

Introduction

This chapter is based on the publication entitled: IR780 based nanomaterials for cancer imaging and photothermal, photodynamic and combinatorial therapies, *International Journal of Pharmaceutics*, 2018, 542 (1-2):164-175.

1. Introduction

Cancer persists as one of the main causes of human death worldwide [1, 2]. In the clinic, surgery, chemotherapy and radiotherapy remain as the gold standard treatments used to treat this disease. However, these conventional therapies have associated several drawbacks, including non-specificity towards cancer cells and impairment by resistance mechanisms [3, 4].

To overcome these problems, new therapeutic approaches are currently under development. In particular, photodynamic therapy (PDT) and photothermal therapy (PTT) have shown promising results in cancer treatment [5-7]. These light-based therapies employ photosensitizers (in PDT) or photothermal agents (in PTT) that upon interaction with light produce reactive oxygen species (ROS) or a temperature increase, respectively [8]. In phototherapies, the use of near-infrared (NIR) photoabsorbers is fundamental since they can interact with NIR light (750-1000 nm) [9]. Such is of paramount importance since NIR radiation displays minimal interactions with biological components (*e.g.* water, collagen, melanin) and a high penetration depth [9]. Thus, when compared to conventional treatments, NIR phototherapies achieve a higher selectivity towards the tumor zone, since only the photoabsorbers accumulated in this zone are activated by NIR light, leading to a reduction of the side effects on healthy tissues [10].

So far, several materials (*e.g.* gold nanorods [11], graphene oxide [12]) and small molecules (*e.g.* Indocyanine Green (ICG) [13], IR780 [14], and MHI-148 [15]) that are capable of interacting with NIR light have been explored for cancer phototherapy. In particular, IR780 based phototherapies have attracted a lot of interest due to the versatility of this small molecule [16, 17].

1.1. IR780: properties, relevance and limitations

IR780 is a prototypic NIR hepthamethine cyanine agent, with a high molar extinction coefficient (2.65 – 3.3 x 10^5 M^{-1} cm^{-1}) [18-21]. This molecule has an absorption peak at 780 nm and can produce a temperature increase and/or ROS upon interaction with NIR light (Figure 1) [22]. Furthermore, IR780 also emits fluorescence with a high intensity in the 807-823 nm wavelength range, which enables its use for imaging applications (Figure 2) [23, 24]. Zhang *et al.* (2010) reported that IR780 can be used to image breast, cervical, lung (Figure 2 C) and osteosarcoma tumors in mice, since the observed fluorescence signals in the tumor after intravenous administration (dose of 0.2 mg/kg) were greatly superior to those observed in the healthy tissues [25]. The preferential tumor accumulation of IR780 was also observed in mice bearing prostate cancer xenografts after intraperitoneal injection (dose of 0.334 mg/kg) [26]. These results seem to be correlated to the fact that IR780 internalization is mediated by organic-anion-transporting polypeptides (OATPs), which are overexpressed in several types of cancer cells [25]. Furthermore, IR780 may also be covalently conjugated with therapeutic molecules

(*e.g.* abiraterone) by modifying the chlorine atom present on IR780 cyclohexenyl ring, which may be a convenient route for the production of IR780 based theragnostics [27].

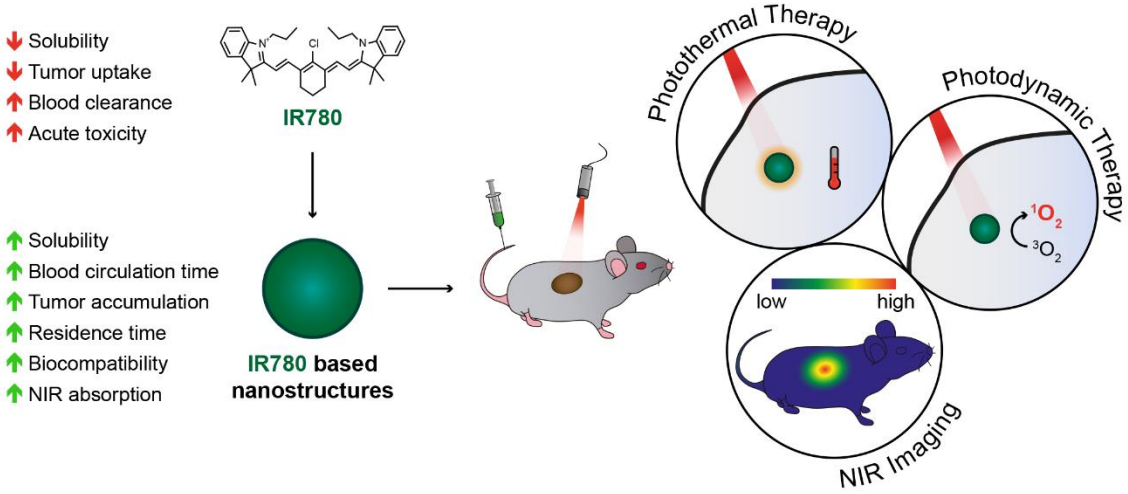

Figure 1. Schematic illustration of IR780 based nanostructures applicability for cancer phototherapy and imaging.

Compared to ICG, a water soluble FDA approved NIR agent, IR780 has a greater photostability and can display a higher fluorescence intensity (Figure 2 B), which are important properties for experiments with repeated NIR imaging sessions [16, 28]. Still, most of the IR780 injected dose is cleared within 24 h, which is not optimal for continuous tumor monitorization [28-30]. On the other hand, ICG has a systemic accumulation and it is cleared within minutes, thus displaying a low tumor tracking ability and a short body-residence that impairs the time-frame for imaging experiments [31]. The performance of IR780 for sentinel lymph node mapping is also superior to that of ICG and quantum dots [16]. Furthermore, the fluorescence efficiency of IR780 is also comparable and in some cases higher than that of other NIR emitting agents (see Table 1 for further details). In this way, the tumor targeting capacity of IR780 together with its high fluorescence efficiency and NIR absorption/emission properties constitute an advantage over other dyes used for cancer imaging (Table 1).

Furthermore, upon interaction with NIR light, IR780 can also produce a temperature increase and/or Singlet Oxygen ($^1O_2$) with high efficiency (Table 1), which can cause cytotoxicity to cells (described in detail in section 1.3). The quantum yield of $^1O_2$ production by IR780 is superior to that of several NIR agents, including ICG (Table 1). However, the direct application of IR780 for cancer PTT and PDT is severely limited since its poor water solubility does not allow the administration of a dose that achieves a tumor accumulation concomitant with the attainment of a suitable therapeutic effect upon NIR laser irradiation [23, 24, 32, 33]. Moreover, the

intravenous administration of high IR780 quantities is also limited by the fact that this NIR agent can induce acute toxicity to mice at doses higher than 1 mg/kg [34, 35].

To address these problems, IR780 can be encapsulated in different types of nanostructures, which improve IR780 solubility and tumor homing capacity since nanomaterials can accumulate in the tumor through passive and/or active targeting mechanisms (further detailed in section 1.2). As importantly, the encapsulation of IR780 in nanostructures can suppress the IR780 induced toxicity [32, 34-36]. In this way, the encapsulation of IR780 in nanostructures can result in enhanced therapeutic and imaging capabilities (further detailed in sections 1.3 and 1.4).

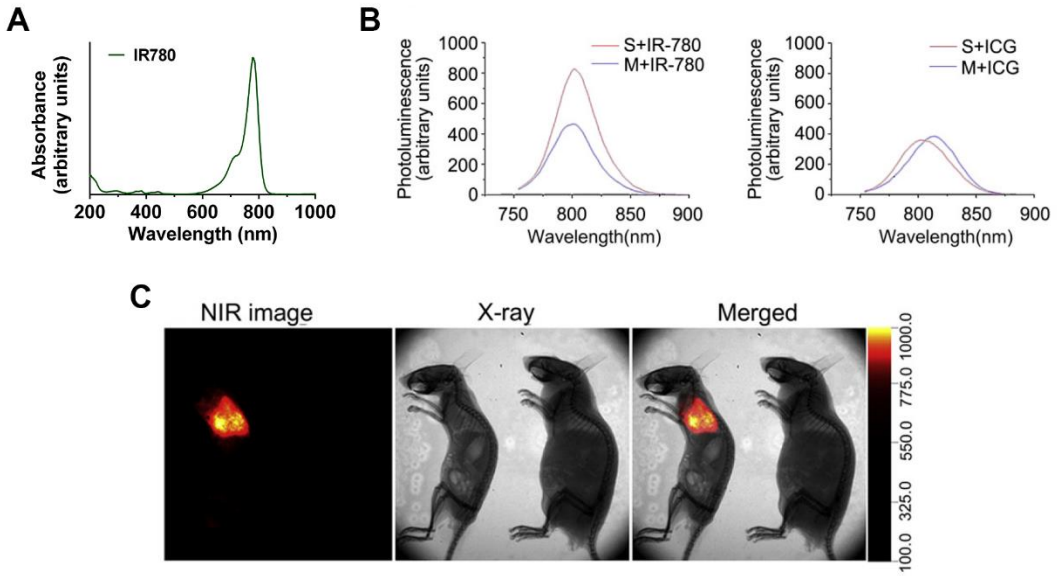

Figure 2. Optical and biological properties of IR780. UV-Vis-NIR spectrum of IR780 in methanol (A). Fluorescence of IR780 in fetal calf serum (S+IR-780) and methanol (M+IR-780, (B)); Fluorescence of ICG in fetal calf serum (S+ICG) and methanol (M+ICG). Reprinted from [16], Copyright (2010), with permission from Elsevier. NIR fluorescence imaging of chemically-induced lung tumor bearing mouse (left) and normal mouse (right) after i.v. injection of IR780 (C). Reprinted from [25], Copyright (2010), with permission from Elsevier.

1.2. IR780 based nanostructures: general considerations

To overcome the limitations of IR780, associated with its low solubility in water (which is below 0.4 μg/mL [35]) and its rapid clearance from the body [30], this molecule has been encapsulated within different types of nanostructures that present a hydrophobic core such as micelles [14, 37, 38], and polymeric [29] or lipid nanoparticles [24, 39]. For instance, the encapsulation of IR780 in Vitamin E based micelles (formulated with D-α-tocopheryl polyethylene glycol succinate (TPGS) and D-α-tocopheryl succinate (TOS)) resulted in a 105- to 115-fold increase in IR780 solubility [14]. Additionally, IR780 can also be conjugated with hydrophilic polymers (*e.g.* poly(ethylene glycol) (PEG) [34], Hyaluronic acid (HA) [40]) or loaded in the hydrophobic regions

of some proteins (*e.g.* Human Serum Albumin (HSA) [35] or Transferrin [41]) in order to improve its solubility.

Moreover, the encapsulation of IR780 in nanostructures has also been used to enhance the accumulation of this molecule in the tumor zone, by taking advantage of the so called Enhanced Permeation and Retention (EPR) effect [29, 40, 42]. The tumor vasculature displays leaky cell-to-cell junctions, and thus the nanostructures can extravasate through these differently sized fenestrae (200-1200 nm), leading to their accumulation at the tumor site [43]. Nanostructures can also be retained in the tumor, since this zone has a defective lymphatic drainage that prevents nanostructures removal [44].

Taking these considerations into account, IR780 based nanostructures must be precisely engineered regarding their size, charge, surface (corona) composition and targeting ligands decoration, since these parameters will dictate the nanostructures' accumulation and penetration into the tumor, as well as their cellular internalization (Figure 3) [9]. Furthermore, these properties have also impacted on nanostructures' blood clearance and off-target accumulation, thus having a critical role on the success of IR780 based phototherapies [45].

In the next sub-sections, general considerations regarding the impact of nanostructures' physico-chemical properties on their biodistribution are provided since these parameters will ultimately influence nanomaterials' theragnostic capacity.

1.2.1. Size

The size of nanomaterials has an important role on nanostructures' blood circulation time and tumor accumulation [9]. Nanomaterials with a size below 5 nm are usually rapidly cleared from circulation through renal filtration, impairing their ability to reach to the tumor site [44, 46]. Furthermore, nanostructures smaller than 50 nm can accumulate in the liver (extravasation through the liver fenestrae that display a size between 50 and 100 nm) [44, 47], and those larger than 200 nm tend to be retained in the spleen and phagocytized by splenic macrophages or by liver Kupffer cells [48]. Taking these size requirements and the EPR effect considerations into account, nanomaterials should have a size comprehended between 100-200 nm to effectively reach the tumor microenvironment [44].

Furthermore, the nanostructures' size influences their tumor penetration capacity and cellular internalization processes [49-51]. Still, it should be noted that each nanostructure tends to display an optimal size for tumor accumulation and cellular internalization, demanding an appropriate optimization of this parameter for every type of formulation.

Table 1. Photo-physical properties of different agents (including NIR agents) used for cancer related applications. Please note that properties vary according to the experimental conditions reported.

Name	λ_{max} (nm)	Molar extinction coefficient (ε; M^{-1} cm^{-1})	Em_{max} (nm)	Fluorescence quantum yield (Φ_f)	Singlet oxygen quantum yield (Φ_{SO})	Optimal interaction with NIR light	Tumor targeting	Ref.
Chlorin e6	654-667*	31000-55000	662-669	0.16-0.18	0.55	N	N	[52-56]
IRDye® 700DX	680-689	165000-210000	687-700	0.14-0.24	0.3	N	N	[57, 58]
IRDye® 800CW	775	240000	795	0.1	-	Y	N	[59-62]
IR780	777-780	265000-330000	798-823	0.07-0.17	0.127	Y	Y	[18-21, 63, 64]
ICG	780-785	115000-204000	812-822	0.012-0.078	0.008	Y	N	[31, 65, 66]
IR783	782	261000	810	0.084	0.007	Y	Y	[66, 67]
MHI-148	785	270000	808	0.12	-	Y	Y	[31]

* Second absorption peak.

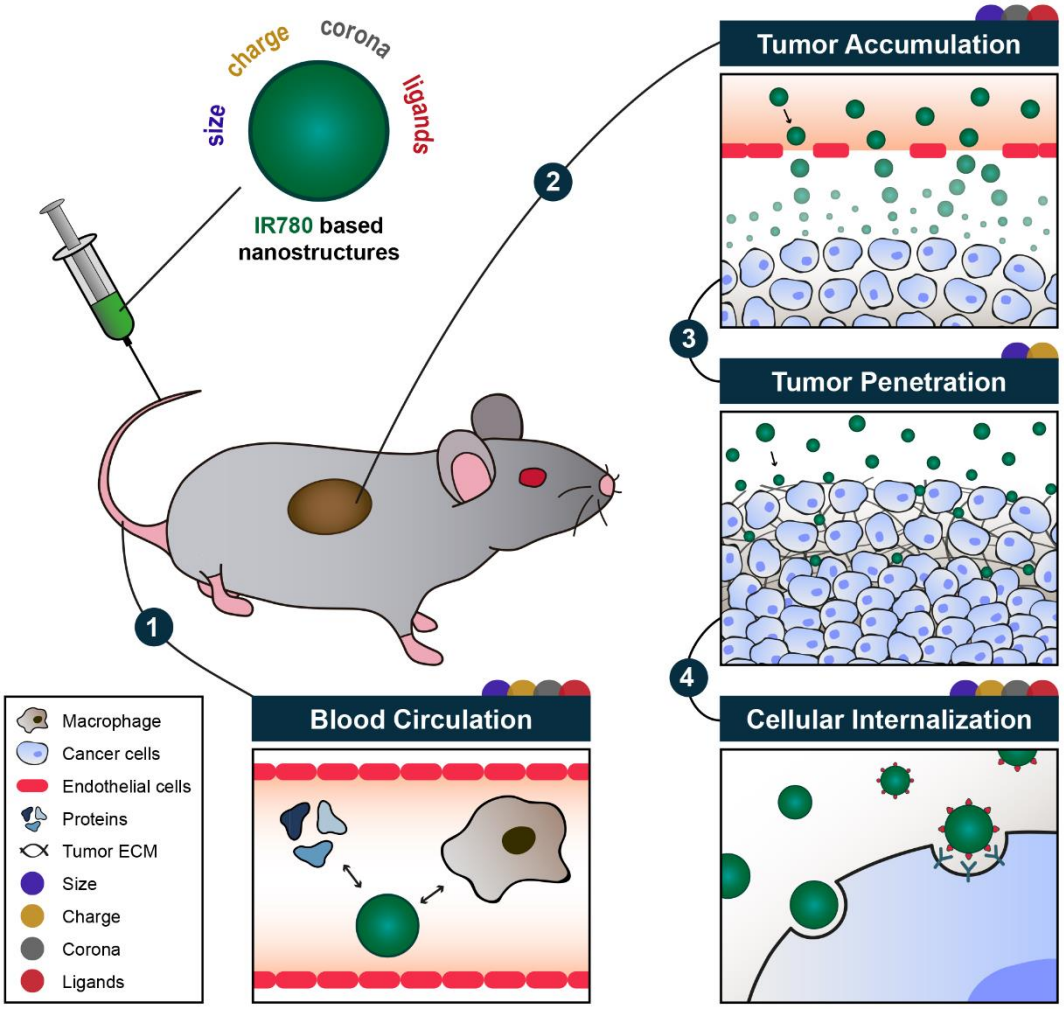

Figure 3. Representation of the different parameters that affect IR780 based nanostructures' blood circulation, tumor accumulation and penetration, and uptake by cancer cells. The colored half-circles indicate the main parameters influencing each phase.

1.2.2. Charge

The charge of nanostructures is another important parameter that must be taken into account, since it affects nanostructures' cellular internalization [68, 69]. In fact, nanomaterials with a positive surface charge usually display a higher uptake by cancer cells, owed to the electrostatic interactions established between the nanomaterial and the negatively charged moieties of cancer cells' membrane (*e.g.* sialic acid or phosphatidylserine) [70].

Neutrally charged (zeta potential between -10 mV and +10 mV) nanomaterials are often considered the most suitable for cancer therapy, since their highly charged equivalents often display i) enhanced opsonization by serum proteins [71], ii) higher uptake by Reticuloendothelial System (RES) cells and liver [72, 73], and iii) diminished tumor penetration capacity due to interaction with the tumor's extracellular matrix (ECM) [74], thus decreasing

the number of nanostructures available to reach the tumor site and become internalized by cancer cells.

1.2.3. Corona

Nanomaterials' corona plays an important role on their blood circulation time and cellular uptake, since it modulates nanomaterials interaction with macrophages and serum proteins [75-77]. In this way, enhancing the blood circulation time of nanostructures can improve their tumor accumulation, since the nanodevices have more chances to benefit from the EPR effect [29].

For this purpose, the functionalization of nanostructures with PEG is the most commonly applied strategy since it can reduce nanomaterials' opsonization and uptake by RES cells/organs [78]. In this regard, Yuan *et al*. (2015) verified that PEG-IR780-C13 micelles display a high tumor accumulation and low uptake by RES organs (liver and spleen) [34]. In contrast, the IR780-C13 conjugates (not PEGylated) demonstrated a higher uptake by the liver, with a non-appreciable tumor accumulation, thus demonstrating the benefits of PEGylation [34]. Still, it should be taken into consideration that in order to profit from PEGylation, an optimization of the PEG molecular weight and the PEG density immobilized on nanostructures' surface is required [79-81]. Furthermore, PEGylation of nanomaterials can also improve their biocompatibility and colloidal stability, which will also dictate their applicability in cancer therapy [34].

Besides PEG, poly(phosphorylcholine) based polymers are also capable of conferring IR780 based nanostructures a high tumor accumulation [28, 29, 42]. Furthermore, the incorporation of IR780 in HSA nanoparticles also results in a high tumor homing capacity [35].

1.2.4. Targeting ligands

In order to improve the selectivity of nanostructures towards cancer cells, ligands that target overexpressed receptors on cancer cell' membranes can be immobilized on nanomaterials' surface. In this regard, folic acid [82], peptides (*e.g*. cyclic Arg-Gly-Asp (cRGD) [83]), proteins (*e.g*. transferrin [41]), aptamers [84] and antibodies (*e.g*. Cetuximab [85]) have been used to functionalize IR780 based nanostructures. For instance, Shih *et al*. (2017) demonstrated that Cetuximab functionalized micelles loaded with IR780 have a higher accumulation in tumors with a high expression of epidermal growth factor receptor (EGFR) than their non-targeted equivalents [85]. In another work, IR780-HA nanoparticles demonstrated a higher uptake by tumors overexpressing CD44 receptors [40].

Nevertheless, it should be taken into account that the ability of targeted nanostructures to improve the tumor uptake and selectivity of cancer therapies depends on the i) ligand density immobilized on nanostructures' surface [86], ii) spacer-arm's length to which the ligand is conjugated [87] and iii) interactions established between serum proteins and the ligand during blood circulation [88, 89].

1.3. IR780 based nanostructures for cancer PTT and/or PDT

IR780 based nanostructures have been applied for cancer phototherapy given their capacity to encapsulate and deliver IR780 to the tumor microenvironment [24]. After the arrival of these nanomaterials to the tumor zone, this site is irradiated and IR780 based nanostructures induce a temperature increase and/or ROS production [14, 34, 40]. The photothermal effect mediated by IR780 based nanostructures can produce different outcomes depending on the temperature variation achieved [9, 90]. In general, the hyperthermia (to 50 °C or above) induced by IR780 irradiation is optimal since such temperature increase elicits irreversible damage to cells, resulting in necrosis [9]. *In vitro*, IR780 based nanostructures have a high capacity to produce $^1O_2$ (type II photosensitization mechanism) upon irradiation, as highlighted in numerous reports [35, 36, 39, 41, 64]. This ROS can in turn affect cells' viability through the oxidation of cellular constituents such as protein, lipids or DNA [91].

In IR780 based phototherapies, radiation with a wavelength of 808 nm is generally used, while the intensity and/or duration varies in order for a suitable therapeutic effect be attained (Tables 2 and 3) [29, 37]. In this context, Han *et al.* (2016) verified that the therapeutic effect mediated by IR780 loaded phosphorylcholine based nanoparticles towards HepG2 cells can be augmented by fine tuning the power density of the radiation (from 0.5 to 0.75 W/cm^2) or the duration of the irradiation process (from 1 to 1.5 min) [29]. In this case, using the optimal conditions (0.5 W/cm^2, 1.5 min), the HepG2 cells viability was reduced by almost 90 % [29]. Moreover, multiple NIR irradiation sessions can also be applied to improve the therapeutic capacity of IR780 based nanostructures [35]. For instance, the photothermal and photodynamic effect mediated by IR780 loaded HSA nanoparticles upon exposure to two NIR laser irradiation sessions produced a reduction of the tumor growth – Figure 4 [35].

Furthermore, the encapsulation of IR780 in nanostructures can result in a red-shift in their absorption, likely due to hydrophobic interactions and/or alterations in solvent polarity, leading to an improved absorption at 808 nm, and consequently to a higher phototherapeutic capacity [14, 24, 28]. For instance, Pais-Silva and co-workers verified that IR780 loaded TPGS-TOS micelles display a 2.4-fold higher absorption at 808 nm in comparison to the free IR780 [14]. Kuang *et al.* (2017) also verified that the incorporation of IR780 in cRGD functionalized solid lipid nanoparticles produces a red-shift in their NIR absorption peak (from 780 to 789 nm) [24]. *In vivo*, the IR780 loaded cRGD functionalized solid lipid nanoparticles encapsulating IR780 displayed a higher tumor uptake than non-targeted IR780 loaded solid lipid nanoparticles and free IR780 [24]. Owing to the improved tumor homing capacity, the IR780 loaded cRGD functionalized solid lipid nanoparticles were able to produce a temperature increase to 52.6 °C when the tumor zone is irradiated, leading to the eradication of mice's tumor when low doses of nanostructures were injected (1 mg/kg of IR780 equivalents; 808 nm, 0.5 W/cm^2, 5 min). In contrast, the PTT mediated by non-targeted IR780 loaded solid lipid nanoparticles and free IR780 only led to a reduction of the tumors' growth, since these conditions only

resulted in temperatures increase to 44.3 and 43.2 °C, respectively. The *in vitro* and *in vivo* phototherapeutic performance of other IR780 based nanostructures is summarized in tables 2 and 3, respectively.

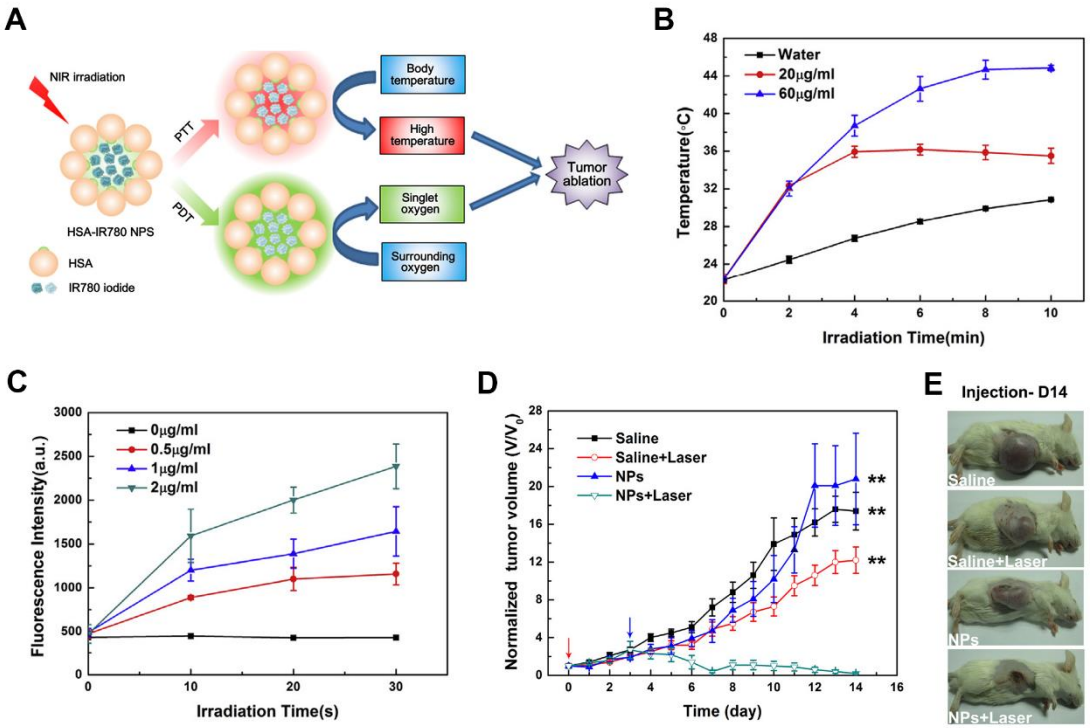

Figure 4. Phototherapeutic capacity of IR780 loaded HSA nanoparticles. Representation of the mechanism of action of IR780 loaded HSA nanoparticles (A). Temperature variation curves of IR780 loaded HSA nanoparticles and water (control) upon exposure to NIR light (B). Fluorescence curves of solutions containing Singlet Oxygen Sensor Green and different concentrations of IR780 loaded HSA nanoparticles upon NIR irradiation (C). Variation of the tumor volume of CT26 tumor bearing mice treated twice with IR780 loaded HSA nanoparticles and NIR radiation (NPs+Laser, (D)). Optical images of the treated mice after 14 days (E). Reprinted from [35], Copyright (2015), with permission from Elsevier.

1.4. IR780 based nanostructures for cancer imaging

The NIR absorption/emission of IR780 and its preferential tumor accumulation enables its use in NIR imaging of tumors with minimal detection of tissues' auto-fluorescence [92]. Despite these promising properties, most of the IR780 injected dose is cleared after intravenous injection within 24 h, which may compromise the time frame for imaging or theragnostic experiments [28-30]. To circumvent this drawback, the encapsulation of IR780 in nanostructures can prolong the residence of this fluorescent dye within mice bodies, thereby allowing tumor monitorization by NIR fluorescence imaging [30, 93, 94]. For instance, fluorescence signals with high intensity could be detected in the tumors of mice for at least 72 h post-administration of IR780 loaded HSA based nanoparticles – Figure 5 A [30]. In contrast,

the groups injected with free IR780 displayed a weak fluorescence intensity after 12 h of administration [30].

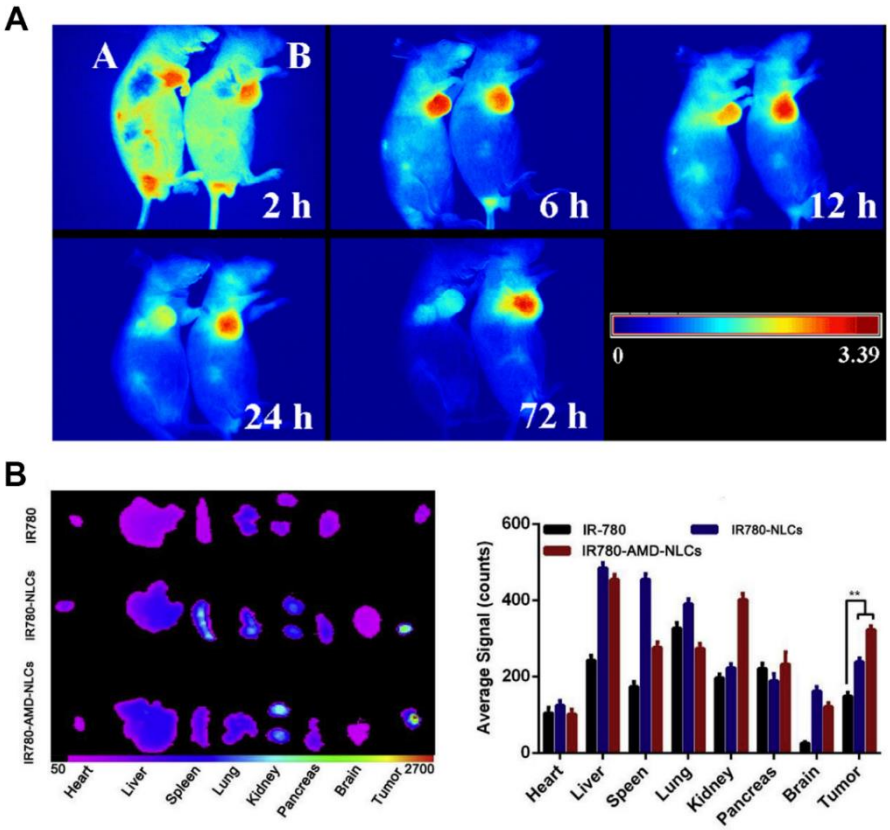

Figure 5. Tumor imaging using IR780 based nanostructures. NIR imaging of BxPC-3 tumor bearing mice injected with IR780 (left mouse) and IR780 loaded HSA-GFLG-Gemcitabine conjugate nanoparticles (right mouse, (A)). Reprinted from [30], Copyright (2017), with permission from Elsevier. *Ex-vivo* imaging of the biodistribution of IR780 loaded AMD3100 coated lipid carriers (IR780-AMD-NLCs), IR780 loaded lipid carriers (IR780-NLCs) and IR780 in 4T1-luc tumor bearing mice (B). Reprinted from [32], Copyright (2017), with permission from Elsevier.

Moreover, IR780 based nanostructures can further improve the detection of mice's tumor since they display a greater intensity in this zone than free IR780, due to their ability to become accumulated within the tumor zone through passive and/or active targeting mechanisms [24, 32, 82, 94]. For instance, the mean NIR fluorescence intensity measured in the tumor zone of IR780 loaded PEGylated liposomes injected mice is ≈ 6-fold higher than that observed in the tumors of mice injected with free IR780 [82]. Li and co-workers verified that IR780 loaded FA-Graphene quantum dots emitted a ≈ 4 times higher NIR fluorescence intensity in mice's tumor than free IR780 [94]. IR780 loaded lipid carriers coated with AMD3100 (CXCR4 receptor targeted) also emitted about 1.35- and 2.18-fold higher fluorescence intensity in tumors than their non-targeted equivalents and free IR780 (Figure 5 B), respectively [32]. Other IR780 based nanomaterials that have been successfully applied for NIR fluorescence imaging of tumor-bearing mice are summarized in table 4.

Table 2. *In vitro* therapeutic performance of IR780 based nanostructures.

IR780 based nanostructures	Phototherapy modality	IR780 concentration	Laser parameters	Other therapeutic agents	Cell line	Cell viability (approx., %)	Ref.
PEG-IR780-C13[a)] micelles	PTT	50 μmol/L	808 nm, 1 W/cm^2, 6 min	-	CT26	2	[34]
IR780 loaded FA-Graphene quantum dots	PTT	30 μg/mL	808 nm, 1 W/cm^2, 5 min	-	HeLa	2	[94]
IR780 and PFH loaded lipid nanoparticles[b)]	PDT	4.18 μg/mL + 12.5 v/v ‰ of PFH	808 nm, 2 W/cm^2, 20 s	PFH	MCF-7	3	[64]
IR780 loaded HSA nanoparticles	PTT/PDT	12.5 μg/mL	808 nm, 1 W/cm^2, 5 min	-	MCF-7	3	[35]
Mitochondria targeted[c)] IR780 loaded liposomes[d)]	PTT/PDT	10 μg/mL	808 nm, 0.8 W/cm^2, 5 min	Lonidamine	LL/2	7	[39]
IR780-HA[e)] nanoparticles	PTT	1.25 μg/mL	808 nm, 1 W/cm^2, 3 min	-	MB-49	8	[40]
IR780 loaded cRGD functionalized solid lipid nanoparticles[f)]	PTT	5.0 μg/mL	808 nm, 0.5 W/cm^2, 5 min	-	U87MG	10	[24]

IR780 loaded Transferrin nanoparticles	PTT/PDT	7.50 μg/mL	808 nm, 1 W/cm^2, 5 min	-	CT26	10	[41]
IR780 and PFH loaded lipid nanoparticles	PDT	8.35 μg/mL + 25.0 v/v ‰ of PFH	808 nm, 2 W/cm^2, 20 s	PFH	CT26	10	[64]
IR780 and DOX loaded liposomes[g)]	PTT	10 μg/mL	808 nm, 0.8 W/cm^2, 5 min	DOX	4T1	10	[22]
IR780 loaded Ce6-HSA conjugate nanoparticles	PTT/PDT	1 μg/mL of Ce6	808 nm, 0.533 W/cm^2, 30 s + 660 nm, 0.04 W/cm^2, 3 min	Ce6	CT26	10	[95]
IR780 loaded PMPC-*b*-PBMA[h)] nanoparticles	PTT	40 μg/mL	808 nm, 0.5 W/cm^2, 1.5 min	-	HepG2	11	[29]
IR780 loaded Heparin-FA nanoparticles	PTT	5 μg/mL	808 nm, 0.6 W/cm^2, 5 min	-	MCF-7	13	[23]
IR780 loaded HA-C18[i)] micelles	PTT	50 μg/mL of micelles	808 nm, 2 W/cm^2, 2 min	-	TC-1	13	[33]

IR780 and PFH loaded lipid nanoparticles	PDT	2.09 μg/mL + 6.25 v/v ‰ of PFH	808 nm, 2 W/cm^2, 20 s	PFH	CT26 (hypoxic conditions)	14	[64]
IR780 loaded PMDPC[j] micelles	PTT	5 μg/mL	808 nm, 0.8 W/cm^2, 5 min	-	BxPC-3	14	[28]
IR780 loaded PEG-*b*-PCL[k] based micelles	PTT	10 μg/mL	808nm, 0.6 W/cm^2, 20 min	-	HCT-116	16	[37]
IR780 and DOX loaded folate targeted bubble generating liposomes[l]	PTT	100 μg/mL of DOX	780 nm, 1 W/cm^2, 15 min	DOX	KB	16	[82]
IR780 loaded TPGS-TOS[m] micelles	PDT	1.5 μg/mL	808 nm, 1.7 W/cm^2, 5 min	TPGS and TOS	MCF-7	20	[14]
IR780 loaded AMD3100 coated lipid carriers[n]	PTT	1.6 μg/mL	808 nm, 1 W/cm^2, 4 min	AMD3100	4T1-luc	21	[32]
IR-780 loaded PMPC-*b*-P(MEMA-hydrazide-DOX)[o] micelles	PTT	2.6 μg/mL + 6.0 μg/mL of DOX	808 nm, 1.5 W/cm^2, 5 min	DOX	MCF-7/ADR	24	[42]
IR780 and siRNA loaded HSA-based nanoparticles[p]	PTT	0.3 μg/well of siRNA	808 nm, 3 W/cm^2, 3 min	Twist siRNA	4T1	26	[96]

HA and PPy coated IR780 loaded PLGA nanoparticles	PTT/PDT	20 μg/mL of PPy	660 nm, 0.2 W/cm^2, 5 min + 808 nm, 2 W/cm^2, 5 min	PPy	MDA-MB-231	30	[97]
HA and PPy coated IR780 loaded PLGA nanoparticles	PTT/PDT	20 μg/mL of PPy	660 nm, 0.2 W/cm^2, 5 min + 808 nm, 2 W/cm^2, 5 min	PPy	SCC-7	31	[97]

[a)] Aliphatic IR780 conjugated with PEG (PEG-IR780-C13); [b)] formulated with Lecithin, Cholesterol and 1,2-distearyl-*sn*-glycero-3-phosphoethanaolamine-N-[methoxypoly-(ethylene glycol)] (DSPE-PEG); [c)] PPh_3Br–$(CH_2)_4$–COOH (TPP); [d)] formulated with 1,2-dipalmitoyl-*sn*-glycero-3-phosphocholine (DPPC), 1,2-distearoyl-*sn*-glycero-3-phosphocholine (DSPC), DSPE-PEG-TPP and Cholesterol; [e)] HA-IR780 conjugate with 4-Aminothiophenol as linkage (IR780-HA); [f)] formulated with Palmitic Acid, p407, Tween 80, DSPE-PEG-COOH and DSPE-PEG-cRGD; [g)] formulated with DPPC, 1-myristoyl-2-palmitoyl-*sn*-glycero-3-phosphocholine (MPPC) and DSPE-PEG; [h)] poly(2-methacryloyloxyethyl phosphorylcholine)-*b*-poly(*n*-butyl methacrylate) (PMPC-*b*-PBMA); [i)] HA conjugated with Octadecyl amine (HA-C18); [j)] poly(12-methacryloyloxy dodecyl phosphorylcholine) (PMDPC); [k)] PEG-*b*-Poly(caprolactone) (PEG-*b*-PCL); [l)] formulated with DPPC, Cholesterol, DSPE-PEG and Ammonium Bicarbonate (NH_4HCO_3); [m)] formulated with TPGS and TOS; [n)] formulated with Phosphatidylcholine, Medium Chain Triglycerides and Trilaurin; [o)] poly(methacryloyloxyethyl phosphorylcholine)-*b*-poly(2-methoxy-2-oxoethyl methacrylate-hydrazide-DOX) (PMPC-*b*-P(MEMA-hydrazide-DOX)); [p)] R9-S-S-DOPE(1,2-dioleoyl-*sn*-glycero-3-phosphoethanolamine) core-HSA shell nanoparticles.

Table 3. *In vivo* therapeutic performance of IR780 based nanostructures.

IR780 based nanostructures	Phototherapy modality	Tumor model	Administration route	Dose	Laser parameters	Other therapeutic molecules	Therapeutic effect	Ref.
IR780 and DOX loaded liposomes	PTT	4T1 tumor bearing mice	i.t.	20 μg of IR780	808 nm, 1 W/cm^2, 5 min	DOX	Tumor eradication	[22]
IR780 loaded cRGD functionalized solid lipid nanoparticles	PTT	U87MG tumor bearing mice	i.v.	1 mg/kg of IR780	808 nm, 0.5 W/cm^2, 5 min	-	Tumor eradication	[24]
IR780 loaded Cetuximab functionalized PEG-*b*-PCL based micelles	PTT	HCT-116 tumor bearing mice	i.v.	1.25 mg/kg of IR780	NIR radiation, 1.8 W/cm^2, 5 min	Cetuximab	Tumor eradication	[85]
IR780 loaded AMD3100 coated lipid carriers	PTT	4T1-luc tumor bearing mice	i.v.	1.4 mg/kg of IR780 0.6 mg/kg of AMD3100	808 nm, 1 W/cm^2, 5 min	AMD3100	Tumor eradication	[32]
Mitochondria targeted IR780 loaded liposomes	PTT/PDT	LL/2 tumor bearing mice	i.v.	1.5 mg/kg of IR780 9 mg/kg Lonidamine	808 nm, 1.8 W/cm^2, 5 min	Lonidamine	Tumor eradication	[39]
IR780-HA nanoparticles	PTT	MB-49 tumor bearing mice	i.v.	5 mg/kg of IR780	808 nm, 1 W/cm^2, 6 min	-	Tumor eradication	[40]

IR780 loaded Ce6-HSA conjugate nanoparticles	PTT/PDT	CT26 tumor bearing mice	i.v.	0.4 mg/kg of Ce6	808 nm, 0.533 W/cm^2, 40 s + 660 nm, 0.04 W/cm^2, 15 min	Ce6	Tumor eradication	[95]
IR780 loaded FA-Graphene quantum dots	PTT	HeLa tumor bearing mice	i.v.	2 mg/kg of nanostructures	808 nm, 1 W/cm^2, 5 min	-	Tumor eradication	[94]
IR780 loaded HA-C18 micelles	PTT	TC-1 tumor bearing mice	i.v.	10 mg/kg of micelles	808 nm, 2 W/cm^2, 2 min	-	Tumor eradication	[33]
IR780 and PFH loaded lipid nanoparticles	PDT	CT26 tumor bearing mice	i.t.	7.8 μg of IR780 30 v/v % of PFH (50 μL)	808 nm, 2 W/cm^2, 10 s (twice)	PFH	Tumor regression	[64]
IR780 loaded PMPC-*b*-P(MEMA-hydrazide-DOX) micelles	PTT	MCF-7 and MCF-7/ADR tumor bearing mice	i.v.	10.5 μg of IR780 23.8 μg of DOX	808 nm, 1.9 W/cm^2, 5 min	DOX	Tumor regression	[42]
IR780 loaded Heparin-FA nanoparticles	PTT	MCF-7 tumor bearing mice	i.v.	1.4 mg/kg of IR780	808 nm, 0.8 W/cm^2, 5 min	-	Tumor regression	[23]
HA and PPy coated IR780 loaded PLGA nanoparticles	PTT/PDT	SCC-7 tumor bearing mice	i.t.	5 mg/kg of PPy	660 nm, 0.2 W/cm^2, 3 min + 808 nm, 2 W/cm^2, 3 min	PPy	Tumor regression	[97]

IR780 and DOX loaded Folate targeted bubble generating liposomes	PTT	KB tumor bearing mice	i.v.	10 mg/kg of DOX	780 nm, 1 W/cm^2, 15 min	DOX	Tumor regression	[82]
IR780 loaded Transferrin nanoparticles	PTT/PDT	CT26 tumor bearing mice	i.v.	20 mg/kg of IR780	808 nm, 1 W/cm^2, 5 min	-	Tumor growth inhibition	[41]
PEG-IR780-C13 micelles	PTT	CT26 tumor bearing mice	i.v.	30 mg/kg of micelles	808 nm, 1 W/cm^2, 10 min	-	Tumor growth inhibition	[34]
IR780 and PFH loaded lipid nanoparticles	PDT	CT26 tumor bearing mice	i.v.	12 μg of IR780 10 v/v % of PFH (200 μL)	808 nm, 2 W/cm^2, 10 s (twice)	PFH	Tumor growth reduction	[64]
IR780 and PFOB loaded CRGDK-PEG-PCL based micelles	PDT	MDA-MB-231 tumor bearing mice	i.v.	20 μg of IR780	808 nm, 2 W/cm^2, 20 sec	PFOB[q)]	Tumor growth reduction	[36]
IR780 and siRNA loaded HSA-based nanoparticles	PTT	4T1 tumor bearing mice	i.v.	0.8 mg/kg of IR780 1.0 mg/kg of siRNA	808 nm, 2.4 W/cm^2, 5 min	Twist siRNA	Tumor growth reduction	[96]
IR780 loaded PEG-*b*-PCL based micelles	PTT	HCT-116 tumor bearing mice	i.v.	1.25 mg/kg of IR780	808 nm, 1.8 W/cm^2, 5 min	-	Tumor growth reduction	[37]
IR780 loaded HSA nanoparticles	PTT/PDT	CT26 tumor bearing mice	i.v. + i.t. (3 days after i.v.)	20 mg/kg of IR780 + 2.5 mg/kg of IR780	808 nm, 1 W/cm^2, 5 min + 808 nm, 2 W/cm^2, 2 min	-	Tumor growth reduction	[35]

[q)] Perfluorooctyl bromide (PFOB).

1.5. IR780 based nanostructures for combination with other molecules or materials

The phototherapeutic effect mediated by IR780 based nanostructures can be improved by combining IR780 with other therapeutic molecules. In this way, an effective therapeutic outcome can be achieved by administering a lower drug dose, by using radiation with a weaker intensity or by employing shorter irradiation sessions.

Nanostructures co-encapsulating IR780 and chemotherapeutic drugs have been investigated for cancer chemo-phototherapy (Tables 2 and 3) [22, 39, 42, 82, 96]. In this regard, Yan *et al*. (2016) prepared IR780 and doxorubicin (DOX) loaded liposomes which after intratumoral injection, were able to induce the eradication of mice's tumor upon irradiation (808 nm, 1 W/cm^2, 5 min) [22]. In contrast, liposomes encapsulating just IR780 (PTT) or DOX (chemotherapy) only promoted a reduction of the tumor growth, which highlights the enhanced efficacy of chemo-phototherapeutic effect mediated by the liposomes encapsulating the IR780-DOX combination [22]. Other therapeutic molecules such as siRNA (Twist siRNA [96]) or antibodies (Cetuximab [85]) also demonstrated a promising therapeutic outcome when they were co-encapsulated in IR780 based nanostructures (Table 3).

The co-delivery of IR780 with oxygen carrying agents can improve the PDT effect mediated by IR780 based nanostructures. In this context, the co-encapsulation of IR780 and perfluorohexane (PFH) in lipid nanoparticles could greatly improve the singlet oxygen produced upon irradiation both in regular and hypoxic conditions [64]. *In vitro,* the IR780 and PFH loaded lipid nanoparticles were able to reduce the viability of different cancer cells (in regular and hypoxic conditions) by more than 90 % using a relatively low IR780 concentration (< 8.35 μg/mL) and a short irradiation time (808 nm, 2 W/cm^2, 20 s). In another study, Pais-Silva encapsulated IR780 in TPGS-TOS micelles, whose photodynamic effect led to a reduction of MCF-7 cells viability to ≈ 20 % using a low concentration of IR780 (1.5 μg/mL) [14]. The therapeutic effect determined in this study may also be correlated with the intrinsic ability of TPGS and TOS to generate ROS [14].

Finally, phototherapies mediated by IR780 based nanostructures can also be enhanced through their combination with other light-responsive agents [95, 97]. In this regard, Tran *et al*. (2017) prepared IR780 loaded poly(lactic-*co*-glycolic acid) (PLGA) nanoparticles, which were coated with HA and Polypyrrole (PPy), being the latter a photothermal agent [97]. By using these materials combination, the nanoparticles containing IR780 and PPy were able to produce *in vitro* a temperature variation of ≈ 42 °C, while those containing only PPy as the photothermal agent (*i.e*. without IR780) only produced a temperature variation of ≈ 34 °C [97]. In another work, Zhang and co-workers verified that IR780 loaded Chlorin e6 (Ce6)-HSA conjugate nanoparticles (Ce6 is a photosensitizer responsive to 660 nm light; this radiation displays lower penetration depth and a higher interaction with off-target components than NIR light, thus

demanding the use of a weaker intensity) are capable of inducing the eradication of mice's tumor under irradiation (808 nm, 0.533 W/cm^2, 40 s + 660 nm, 0.040 W/cm^2, 15 min) [95]. In contrast, nanostructures exposed to light with a wavelength suitable for only one of the molecules (*i.e*. 808 nm laser light for IR780 or 660 nm laser light for Ce6) just mediated a reduction of the tumor growth [95].

Table 4. Application of IR780 based nanostructures for *in vivo* NIR fluorescence tumor imaging.

IR780 based nanostructures	Tumor model	Administration route	Dose of IR780	Ref.
Free IR780	MCF-7 tumor bearing mice	i.v.	0.2 mg/kg	[25]
Free IR780	HeLa tumor bearing mice	i.v.	0.2 mg/kg	[25]
Free IR780	MG-63 tumor bearing mice	i.v.	0.2 mg/kg	[25]
Free IR780	Chemically-induced lung tumor bearing mice	i.v.	0.2 mg/kg	[25]
Free IR780	PC-3 tumor bearing mice	i.p.	0.334 mg/kg	[26]
IR780 loaded silica cross-linked Pluronic F-127 micelles	A431 tumor bearing mice	i.v.	0.25 μg	[93]
IR780 loaded PMPC-*b*-P(MEMA-hydrazide-DOX) micelles	MCF-7 and MCF-7/ADR tumor bearing mice	i.v.	7.5 μg	[42]
IR780 and PFH loaded lipid nanoparticles	CT26 tumor bearing mice	i.v.	12 μg	[64]
IR780 loaded PMPC-*b*-PBMA nanoparticles	KB tumor bearing mice	i.v.	20 μg	[29]
IR780 loaded ANG/GS/PLGA$^{r)}$ nanoparticles	U87MG tumor bearing mice	i.v.	0.2 mg/kg	[98]
IR780 loaded HSA nanoparticles	CT26 tumor bearing mice	i.v.	0.2 mg/kg	[35]
IR780 loaded Transferrin nanoparticles	CT26 tumor bearing mice	i.v.	0.3 mg/kg	[41]
IR780 loaded AMD3100 coated lipid carriers	4T1-luc tumor bearing mice	i.v.	0.3 mg/kg	[32]
IR780 loaded CPT-ss-Ara-C$^{s)}$ nanoparticles	B16F10 tumor bearing mice	i.v.	0.5 mg/kg	[99]
IR780 loaded PMDPC micelles	BxPC-3 tumor bearing mice	i.v.	0.5 mg/kg	[28]
IR780 loaded Methionine$_{14}$-Lysine$_{22}$- micelles	NCI-H460 tumor bearing mice	i.v.	0.6 mg/kg	[100]

IR780 loaded Methionine$_{14}$-Lysine$_{22}$-PEG micelles	NCI-H460 tumor bearing mice	i.v.	0.6 mg/kg	[100]
IR780 loaded Methionine$_{14}$-Lysine$_{22}$-PLGLAG-PEG micelles	NCI-H460 tumor bearing mice	i.v.	0.6 mg/kg	[100]
IR780 loaded Heparin-FA nanoparticles	MCF-7 tumor bearing mice	i.v.	0.7 mg/kg	[23]
IR780 loaded Ce6-HSA conjugate nanoparticles	CT26 tumor bearing mice	i.v.	0.7 mg/kg	[95]
IR780 and siRNA loaded HSA-based nanoparticles	4T1 tumor bearing mice	i.v.	0.8 mg/kg	[96]
Mitochondria targeted IR780 loaded liposomes	LL/2 tumor bearing mice	i.v.	1 mg/kg	[39]
PEG-IR780-C13 micelles	CT26 tumor bearing mice	i.v.	1 mg/kg*	[34]
IR780 loaded HSA-GFLG-Gemcitabine conjugate nanoparticles	BxPC-3 tumor bearing mice	i.v.	1 mg/kg	[30]
IR780 loaded cRGD functionalized solid lipid nanoparticles	U87MG tumor bearing mice	i.v.	1 mg/kg	[24]
IR780 loaded Cetuximab functionalized PEG-*b*-PCL based micelles	HCT-116 tumor bearing mice	i.v.	1.25 mg/kg*	[85]
IR780 loaded PEG-*b*-PCL based micelles	HCT-116 tumor bearing mice	i.v.	1.25 mg/kg	[37]
IR780 loaded DSPE-PEG micelles	4T1 tumor and metastasis bearing mice	i.v.	1.5 mg/kg	[38]
IR780 loaded FA-Graphene quantum dots	HeLa tumor bearing mice	i.v.	2 mg/kg*	[94]
IR780 loaded HA-C18 micelles	TC-1 tumor bearing mice	i.v.	10 mg/kg*	[33]

* This value corresponds to a dose of IR780 based nanostructures; [r)] Angiopep-2 and PEG functionalized gold coated PLGA (ANG/GS/PLGA); [s)] Camptothecin-Cytarabine conjugate with a disulfide linker (CPT-ss-Ara-C).

1.6. Aims

The main objective of this thesis was to produce Hyaluronic acid-based polymeric micelles encapsulating IR780 and Doxorubicin for application in targeted chemo-phototherapy and imaging of breast cancer cells.

The specific aims of this master's thesis are:

- Development of a Hyaluronic acid-based amphiphilic polymer;
- Formulation of micelles loaded with IR780 and with the IR780-Doxorubicin combination;
- Characterization of the physicochemical properties of both formulations;
- Evaluation of the NIR absorption and photothermal capacity of the micelles;
- Determination of the cytocompatibility of the micelles;
- Investigation of micelles' capacity to target breast cancer cells;
- Evaluation of micelles' phototherapeutic capacity towards breast cancer cells.

Chapter 2

Materials and Methods

2. Materials and Methods

2.1. Materials

Michigan Cancer Foundation-7 (MCF-7) cell line and Normal Human Dermal Fibroblast (NHDF) were obtained from ATCC (Middlesex, UK) and Promocell (Heidelber, Germany), respectively. Fetal bovine serum (FBS) was acquired from Biochrom AG (Berlin, Germany). 1-Ethyl-3-(3'-dimethylaminopropyl)carbodiimide (EDC) was purchased from Merck (Darmstadt, Germany). DOX and HA Sodium Salt (8000-15000 Da) were obtained from Carbosynth (United Kingdom). Acetone, Dimethyl Sulfoxide (DMSO) and methanol were acquired from Fisher Scientific (Oeiras, Portugal). Cell imaging plates were obtained from Ibidi GmbH (Ibidi, Munich, Germany). Cell culture plates and T-flasks were purchased from Thermo Fisher Scientific (Porto, Portugal). Dulbecco's Modified Eagle's Medium F12 (DMEM-F12), IR780 iodide, *N*-Hydroxysuccinimide (NHS), paraformaldehyde, Poly(maleic anhydride-*alt*-1-octadecene) (PMAO; average Mn 30,000-50,000 Da), resazurin and trypsin were bought from Sigma-Aldrich (Sintra, Portugal). Water used in all experiments was double deionized (0.22 μm filtered, 18.2 MΩ cm).

2.2. Methods

2.2.1. Formulation of IR-HPM and IR/DOX-HPM

HA-based Polymeric Micelles (HPM) loaded with IR780 and DOX (IR/DOX-HPM) were prepared through the nanoprecipitation method as previously described by our group [14]. In brief, 1 mL of a Water:Acetone solution (1:1 (v/v)) containing HA grafted PMAO (HA-*g*-PMAO) (5 mg mL^{-1}; the synthesis of HA-*g*-PMAO is described in the Appendix), IR780 (125 μg) and DOX (125 μg) was added dropwise into water under stirring. After 2 h, the aqueous solution was recovered and dialyzed against water (1000 Da cut-off membrane; 2 h), yielding IR/DOX-HPM. The same protocol was used to prepare IR-HPM (using 250 μg of IR780).

2.2.2. Physicochemical characterization of IR-HPM and IR/DOX-HPM

HPM size distribution and zeta potential were evaluated by Dynamic Light Scattering (DLS) in a Zetasizer Nano ZS (Malvern Instruments Ltd., Worcestershire, UK). Transmission Electron Microscopy (TEM) was used to analyse the morphology of both HPM. For such, the nanoformulations were stained with phosphotungstic acid (2 % (w/v)) and were imaged in a Hitachi-HT7700 transmission electron microscope (Hitachi Ltd., Tokyo, Japan), at an accelerating voltage of 100 kV.

2.2.3. Encapsulation Efficiency and Loading Content of IR780 and DOX

HPM ability to encapsulate IR780 and/or DOX was determined by UV-Vis absorption and fluorescence spectroscopies. First HPM were freeze dried in a ScanVac CoolSafe (LaboGene ApS, Lynge, Denmark), and then were resuspended in methanol. Then a standard curve of IR780 (in methanol) and samples' absorbance at 780 nm were used to determine the content of IR780

within the sample, using an Evolution 201 UV-Visible spectrophotometer (Thermo Fisher Scientific Inc., Massachusetts, USA). In turn, the fluorescence emitted by the samples at 590 nm (λ_{ex} = 488 nm) and a standard curve of DOX (in methanol, λ_{ex} = 488 nm, λ_{em} = 590 nm) were employed to determine the content of DOX by using a Spectramax Gemini EM spectrofluorometer (Molecular Devices LLC, California, USA). HPM Encapsulation Efficiency (EE) and Loading Content (LC) were determined according to equations 1 and 2:

$$EE\ (\%) = \frac{Weight\ of\ IR780\ or\ DOX\ encapsulated\ in\ HPM}{Weight\ of\ IR780\ or\ DOX\ initially\ fed} \times 100 \qquad \text{(Eq. 1)}$$

$$LC\ (\%) = \frac{Weight\ of\ IR780\ or\ DOX\ encapsulated\ in\ HPM}{Weight\ of\ loaded\ HPM} \times 100 \qquad \text{(Eq. 2)}$$

2.2.4. NIR Absorption and photothermal capacity of HPM

The ability of IR-HPM and IR/DOX-HPM to interact with NIR light was evaluated by measuring the samples' absorbance in the 750-1000 nm wavelength range. For such, the absorption of IR-HPM and IR/DOX-HPM in water and in methanol after freeze-drying was determined (2.5 μg mL^{-1} of IR780 equivalents). The photothermal capacity of HPM was characterized by evaluating the temperature variations induced by these nanoformulations (at different concentrations of IR780) during 5 min of NIR laser irradiation (808 nm, 1.7 W cm^{-2}). Temperature measurements were performed using a thermocouple thermometer. Water was used as a control.

2.2.5. Cytocompatibility of IR-HPM

The cytocompatibility of IR-HPM towards MCF-7 (breast cancer cell model) and NHDF (normal cell model) was determined using the resazurin method, as previously described by our group [12]. For the assay, cells were seeded (1 x 10^4 cells/well) in 96 well-plates and were cultured in DMEM-F12 medium supplemented with 10 % (v/v) FBS and 1 % (v/v) streptomycin/gentamycin in an incubator with a humidified atmosphere (37 °C, 5 % CO_2). After 24 h, the culture medium was removed and cells were incubated with fresh medium containing different concentrations of IR-HPM. After 24 and 48 h of incubation, the medium was replaced with fresh culture medium containing resazurin (10 % (v/v)) and cells were incubated for 4 h in the dark (37 °C, 5 % CO_2). Then, the fluorescence of resorufin (λ_{ex} = 560 nm; λ_{em} = 590 nm) was measured (Spectramax Gemini EM spectrofluorometer) in order to determine cells' viability. Cells solely incubated with medium and cells incubated with ethanol (70 % (v/v)) were used as negative (K-) and positive (K+) controls, respectively.

2.2.6. Targeting capacity of IR-HPM and IR/DOX-HPM

The targeting capacity of HPM was assessed by investigating their uptake by MCF-7 cells (CD44 overexpressing cells [101-103]) and NHDF (which do not overexpress CD44 [104, 105]) through Confocal Laser Scanning Microscopy (CLSM) and by taking advantage from the intrinsic fluorescence of IR780. In brief, cells were seeded in µ-slide 8-well imaging plates (Ibidi GmbH, Munich, Germany) at a density of 1.5 $x10^4$ cells/well. After 48 h, cells were incubated with culture medium containing HPM (1.5 µg mL^{-1} of IR780 equivalents) and free IR780 (1.5 µg mL^{-1}) during 4 h. Afterwards, the medium was discarded and cells were washed several times with Phosphate Buffered Saline (PBS) solution. Then, cells were fixed with paraformaldehyde 4 %, for 15 min at room temperature and washed twice with the PBS solution. Fluorescence images were acquired using a $\lambda_{ex}/\lambda_{em}$ of 633/650-759 nm in a Zeiss LSM 710 confocal microscope (Carl Zeiss AG, Oberkochen, Germany).

2.2.7. Phototherapeutic effect mediated by HPM

The phototherapeutic capacity of HPM was determined using the resazurin method as described above. In brief, MCF-7 cells were seeded at 1 × 10^4 cells/well in 96-well plates. After 24 h, the medium was replaced by fresh medium containing IR-HPM (IR780: 2 or 3.5 µg mL^{-1}) or IR/DOX-HPM (IR780/DOX: 2/1.10 µg mL^{-1} or 3.5/1.93 µg mL^{-1}). After 4 h of incubation, cells were irradiated with NIR light (808 nm, 1.7 W cm^{-2}) for 5 min. After 24 h of incubation, cells' viability was evaluated. Cells solely incubated with medium and cells incubated with ethanol (70 % (v/v)) were used as negative (K-) and positive (K+) controls, respectively.

2.2.8. Statistical analysis

To compare different groups, one-way analysis of variance (ANOVA) was used with the Student-Newman-Keuls test. A *p* value lower than 0.05 ($p < 0.05$) was considered statistically significant. All data are presented as the mean ± standard deviation (S.D.).

Chapter 3

Results and Discussion

3. Results and Discussion

3.1. Formulation and characterization of IR-HPM and IR/DOX-HPM

The hydrophobicity and non-specific toxicity of IR780 and DOX may limit their application in cancer chemo-phototherapy [106, 107]. In this way, the amphiphilic polymer HA-*g*-PMAO was synthesized in order to be explored in the formulation of novel micelles that can be used in the co-encapsulation of IR780 and DOX (characterization of HA-*g*-PMAO is reported in the Appendix - Figures 14-16). Furthermore, HA-*g*-PMAO micelles may enable a selective cancer cell therapy, mediated by the binding of the HA to the CD44 receptors, which are overexpressed on cancer cells' membrane (Figure 6 A).

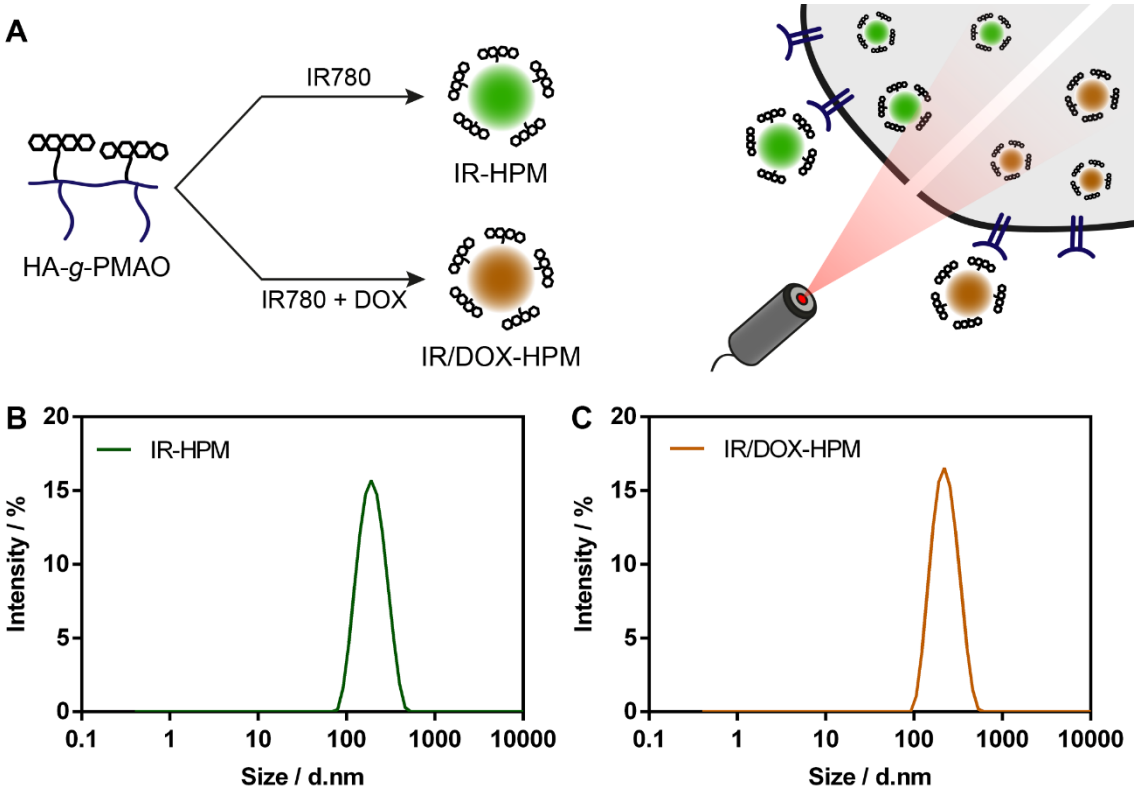

Figure 6. Characterization of HPM physicochemical properties. Schematic representation of HPM assembly and application in cancer therapy (A). DLS size distribution of IR-HPM (B) and IR/DOX-HPM (C).

HA-*g*-PMAO micelles encapsulating IR780 (IR-HPM) were prepared through a nanoprecipitation method, revealing an average size of 173.5 ± 8.5 nm (n=3; batch triplicates; Figure 6 B). The inclusion of the IR780-DOX combination in HA-*g*-PMAO micelles (IR/DOX-HPM) increased slightly the micelles' size to 198.9 ± 2.8 nm (n=3; batch triplicates; Figure 6 C). The differences in the sizes of both formulations may be explained by the different hydrophobic interactions established within the micelles' core. Nevertheless, the size of IR-HPM and IR/DOX-HPM is

within the 100-200 nm range, suggesting their ability to passively accumulate in the tumor zone through the EPR effect [44]. Furthermore, the DLS analysis also revealed that IR-HPM and IR/DOX-HPM present very low polydispersity index (PDI) values of 0.139 ± 0.026 and 0.119 ± 0.028, respectively. Such finding indicates that micelles have a monodisperse size distribution, further corroborating the efficiency of the nanoprecipitation method in the assembly of micelles with suitable physicochemical properties for application in cancer therapy. Additionally, IR-HPM and IR/DOX-HPM presented a zeta potential of -31.3 ± 3.8 mV and -31.9 ± 0.4 mV, respectively. These values are in agreement with those reported in the literature for HA-based micelles [108, 109].

TEM analysis was also performed to characterize the morphology of IR-HPM and IR/DOX-HPM, demonstrating that both formulations have a spherical shape (Figure 7). This morphology may be advantageous since spherical-shaped nanomaterials have been associated with augmented cellular internalization and suitable tumor homing capacity [110].

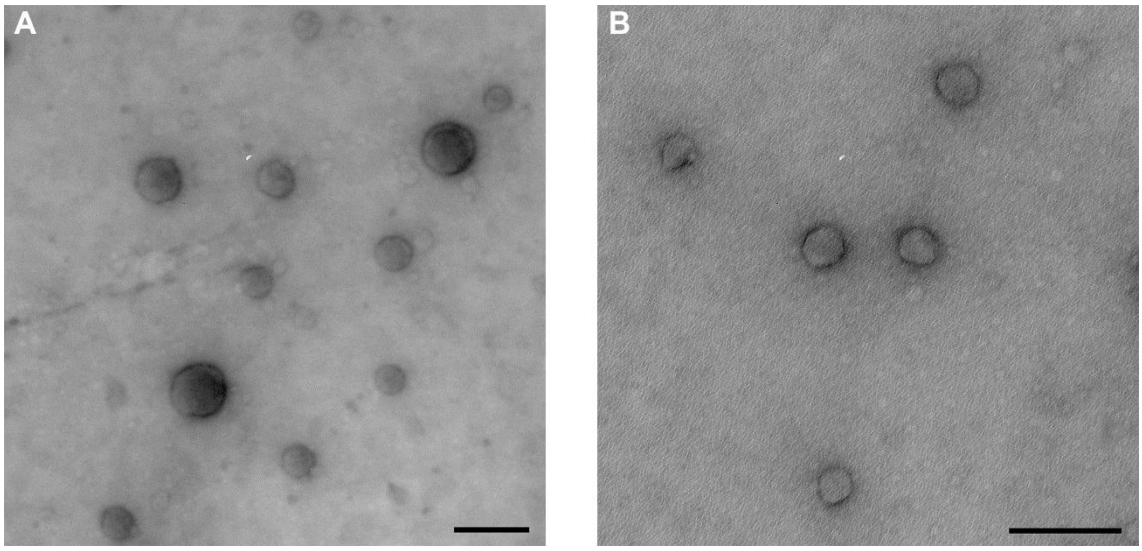

Figure 7. TEM analysis of IR-HPM (A) and IR/DOX-HPM (B). Scale bars correspond to 200 nm.

The HPM micelles presented a similar efficiency in the encapsulation of IR780 (Figure 8 A). In fact, IR780 encapsulation in HPM could increase its water solubility up to 42.15-fold (the water solubility of IR780 is below 0.4 μg mL^{-1} [35, 94]). The IR/DOX-HPM were also capable of encapsulating DOX (Figure 8 A). The loading content of IR-HPM and IR/DOX-HPM is also in line with those of polymeric micelles (Figure 8 B) [103, 111].

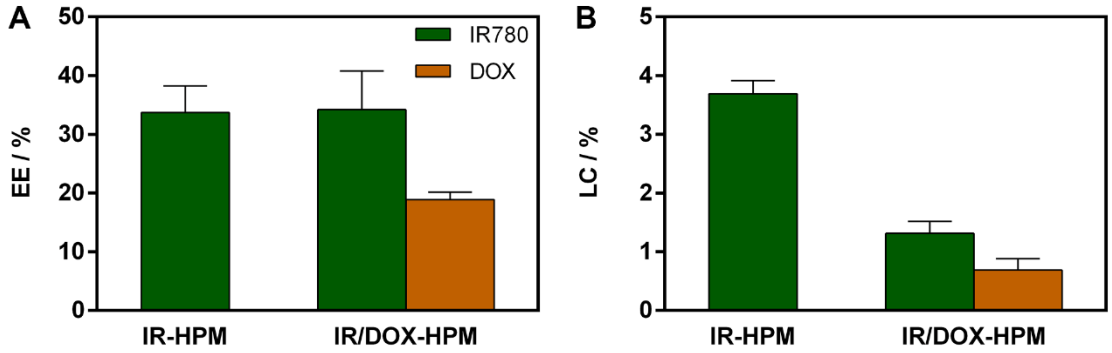

Figure 8. Encapsulation Efficiency (A) and Loading Content (B) of IR780 and/or DOX in IR-HPM and IR/DOX-HPM. Each bar represents mean ± S.D. (n=3; batch triplicates).

3.2. NIR absorption and phototherapeutic capacity of IR-HPM and IR/DOX-HPM

The NIR absorption of IR-HPM and IR/DOX-HPM was then characterized to assess their ability to interact with NIR light. Free IR780 (dissolved in methanol) had a high absorption in the NIR region, revealing a maximum absorption peak at 780 nm (Figure 9). The encapsulation of IR780 in HPM produced a red-shift in its absorption (Figure 9 A). Due to this phenomenon, IR-HPM and IR/DOX-HPM possessed a 2.2-fold higher absorption at 808 nm than free IR780, indicating that these micelles interact with 808 nm radiation, which will be used in photothermal studies. Considering that the NIR absorption spectra of disrupted IR-HPM and IR/DOX-HPM dissolved in methanol and free IR780 were similar (Figure 9 B), the red-shift observed is likely to be a result from alterations in solvents' polarity or from hydrophobic-hydrophobic interactions occurring in micelles' core. This red-shift of IR780 absorption, when encapsulated in polymeric micelles, was also reported by other research groups [14, 35, 41, 112].

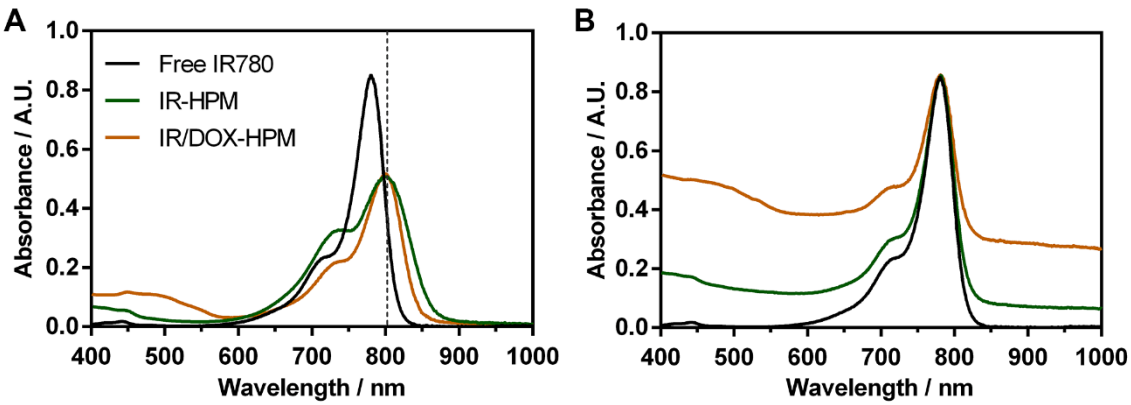

Figure 9. Characterization of HPM optical properties. Absorption spectra of IR-HPM and IR/DOX-HPM (2.5 μg mL^{-1} of IR780 equivalents) in water (A) and in methanol after freeze-drying (B). The spectrum of free IR780 (2.5 μg mL^{-1}) in methanol was also acquired (A-B).

Afterward, the capacity of IR-HPM and IR/DOX-HPM to convert NIR radiation into heat was investigated (Figure 10). For such, HPM at different concentrations of IR780 were irradiated with 808 nm light during 5 min and the temperature changes were recorded (Figure 10). For both formulations, the maximum temperature increase was achieved after 1 min of irradiation (Figure 10). This photothermal behaviour has been associated with the photodegradation of IR780 by NIR light [14, 22, 34, 113]. Moreover, the temperature variations induced by both formulations were similar, suggesting that the differences on HPM physicochemical properties do not affect their photothermal capacity.

At the concentration of 10 μg mL^{-1} (of IR780 equivalents), IR-HPM and IR/DOX-HPM induced a temperature increase of 10 °C (Figure 10). Such temperature variation can induce cellular damages, leading to cancer cells death [90]. On the other hand, HPM produced a photoinduced heat of 4-5 °C at lower concentrations (2 and 3.5 μg mL^{-1} of IR780 equivalents), which can still sensitize cancer cells to other therapeutics [9]. As importantly, the NIR radiation did not induce a significant temperature increase to water (control), which is in agreement with the weak interaction of 808 nm light with water.

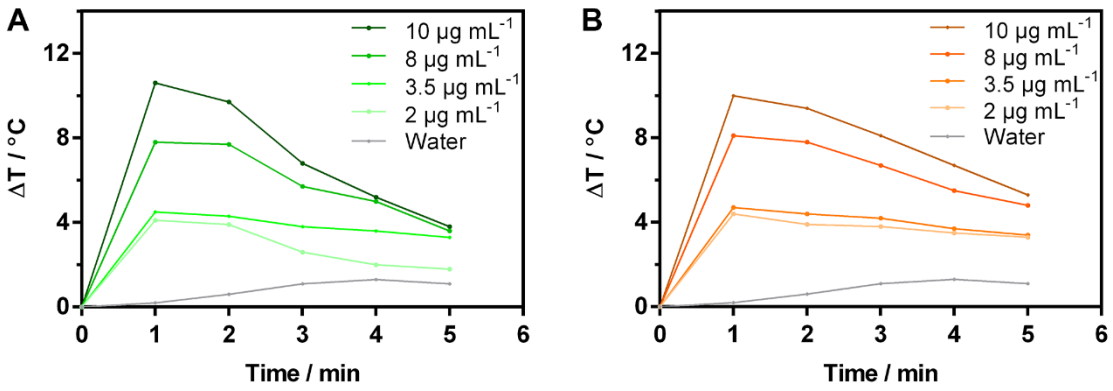

Figure 10. Characterization of HPM photothermal properties. Photoinduced heat produced by IR-HPM (A) and IR/DOX-HPM (B) during 5 min of irradiation (808 nm, 1.7 W cm^{-2}).

In comparison to previous studies, IR-HPM and IR/DOX-HPM were able to produce a photoinduced heat (808 nm, 1.7 W cm^{-2}) of 10 °C at 10 μg mL^{-1} (of IR780 equivalents), while poly(phosphorylcholine)-based micelles encapsulating IR780 induced a similar temperature increase, but required a 4-times higher concentration (40 μg mL^{-1} of IR780 equivalents; 808 nm, 1 W cm^{-2}) [29]. In another report, α-Lipoic acid stabilized IR780 micelles [114] also required a 2-times higher concentration (20 μg mL^{-1} of IR780 equivalents) and a greater power density (2.5 W cm^{-2}) to induce a maximum temperature variation similar to that produced by IR780 loaded HPM (at 10 μg mL^{-1} of IR780 equivalents). Together, these results confirm the photothermal capacity of IR-HPM and IR/DOX-HPM.

3.3. Cytocompatibility of IR-HPM

The encapsulation of IR780 in nanostructures can address the acute-toxicity associated with the administration of free IR780 [106]. In a previous work, we reported that the IC_{50} of IR780 towards MCF-7 cancer cells is about 10.4 μg mL^{-1} [14]. Herein, we investigated the toxicity of IR-HPM towards MCF-7 cells and NHDF, as models of breast cancer and healthy cells respectively (Figure 11). IR-HPM did not induce meaningful variations in MCF-7 and NHDF cells' viability up to 175 μg mL^{-1} of nanostructures (corresponds to an IR780 concentration of 6.88 μg mL^{-1}) (Figure 11 A and B). Therefore, IR780 encapsulation in HPM results in an improved cytocompatibility, a factor that is crucial for the application of these nanoformulations in cancer therapy. Moreover, the cytocompatibility of IR-HPM towards both cells lines also gives a good indication that these nanoformulations may perform an on-demand therapy upon NIR laser irradiation.

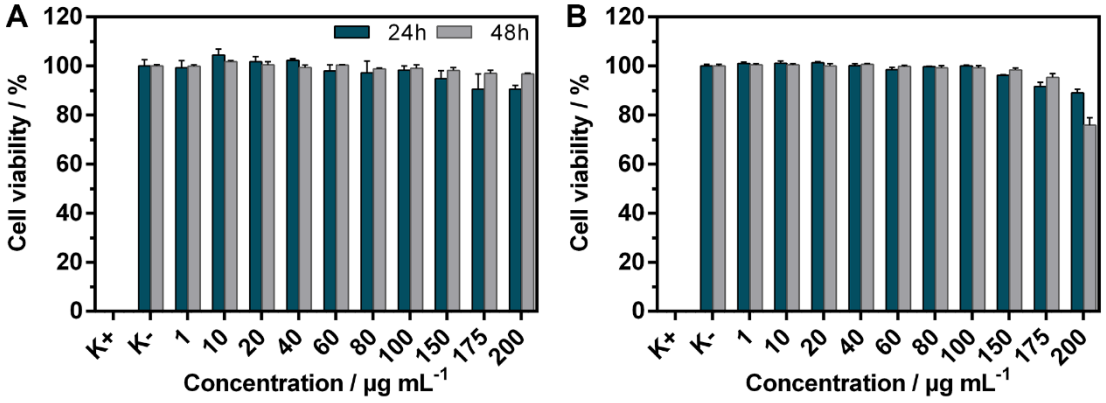

Figure 11. Evaluation of the cytocompatibility of IR-HPM. MCF-7 cells (A) and NHDF (B) were incubated with different concentrations of IR-HPM during 24 and 48 h. K- represents the negative control and K+ the positive control. Each bar represents the mean ± S.D. (n=5).

3.4. Cellular uptake and targeting capacity of IR-HPM and IR/DOX-HPM

After confirming the cytocompatibility of IR-HPM, the selectivity of HPM nanoformulations towards cancer cells was also assessed. For such, the intrinsic fluorescence of IR780 was explored to investigate the internalization of IR-HPM and IR/DOX-HPM by MCF-7 cells (CD44 overexpressing cells [101-103]) and NHDF (which do not overexpress CD44 [104, 105]) through CLSM. The data revealed that MCF-7 cells show fluorescence signals with a higher intensity when compared to NHDF (Figure 12). Furthermore, cells treated with free IR780 displayed fluorescence signals with a weaker intensity (Figure 12). The low uptake of IR780 by cells when not encapsulated in nanomaterials was also observed in a previous report [14]. These results suggest that HPM have a preferential internalization by MCF-7 cells, presumably mediated by

the binding of the HA present on micelles' corona to the CD44 receptors overexpressed on this cell line [101-103]. Cho *et al*. produced HA-based nanomedicines that also displayed a higher internalization by MCF-7 cells [102]. Therefore, the preferential internalization of HPM by MCF-7 cells suggests that this formulation can be used for NIR imaging of breast cancer cells and that it may be able to perform a selective phototherapy.

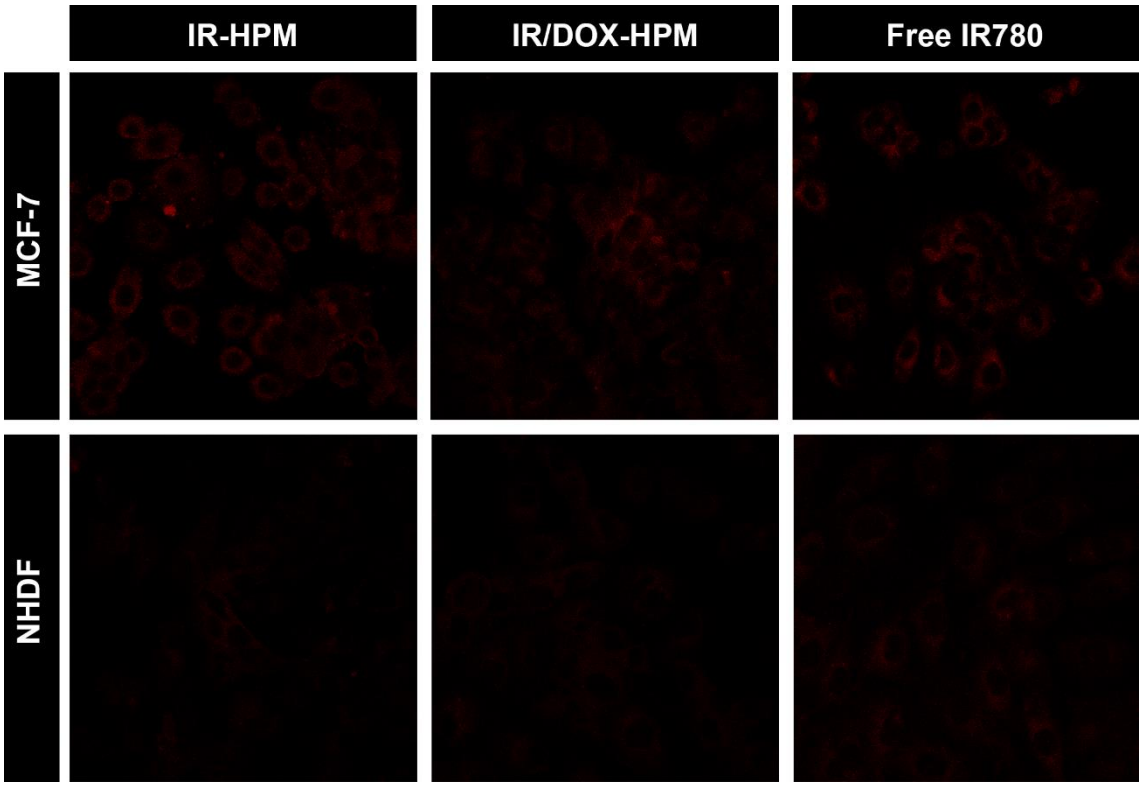

Figure 12. Determination of HPM targeting capacity. Cellular uptake of free IR780, IR-HPM and IR/DOX-HPM by MCF-7 cells and NHDF. Red channel: IR780.

3.5. Phototherapeutic effect mediated by IR-HPM and IR/DOX-HPM

After confirming the preferential uptake of IR-HPM and IR/DOX-HPM by MCF-7 cells, their phototherapeutic capacity was evaluated (Figure 13 A). At the highest concentration tested (3.5 μg mL^{-1} of IR780 equivalents), the combined application of NIR light and IR-HPM induced a reduction on cancer cells' viability to about 59 % (Figure 13 B). Taking into account that non-irradiated IR-HPM and the NIR radiation did not induce meaningful alterations on MCF-7 cells' viability (Figure 13 B), these results confirm that IR-HPM can induce an on-demand phototherapeutic effect.

Furthermore, IR/DOX-HPM produced a reduction of MCF-7 cells' viability to about 66 % (3.5 μg mL^{-1} of IR780; 1.93 μg mL^{-1} of DOX). Moreover, when IR/DOX-HPM were irradiated with NIR light, a viability reduction to about 20 % was attained (Figure 13 B). This outcome is likely to result from a synergic effect between DOX and IR780 (that is responsible for a temperature increase and/or reactive oxygen species production), and thus confirm the potential of the chemo-phototherapy mediated by IR/DOX-HPM.

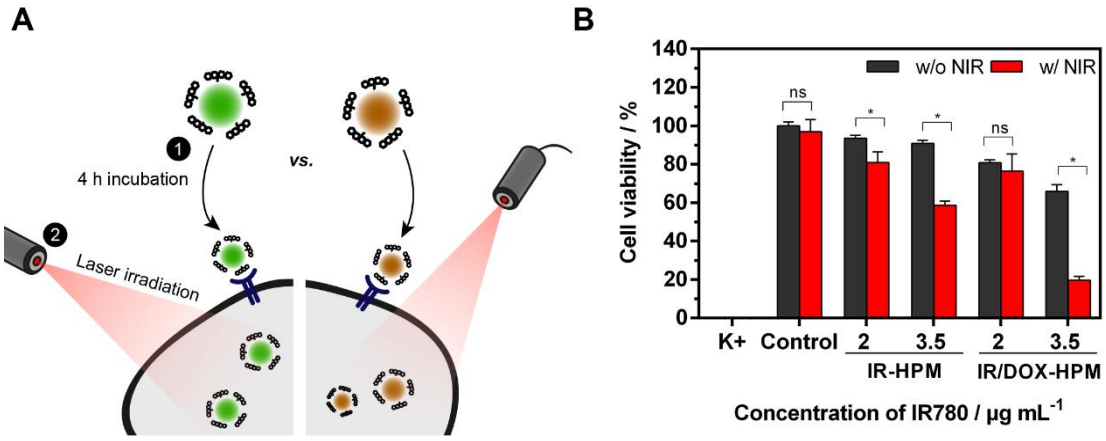

Figure 13. Determination of the therapeutic capacity of IR-HPM and IR/DOX-HPM. Schematic representation of the procedure used to evaluate the phototherapeutic effect of IR-HPM or IR/DOX-HPM towards MCF-7 cells (A). Therapeutic effect mediated by HPM towards MCF-7 cells without (w/o NIR) and with NIR (w/ NIR) laser irradiation (808 nm, 1.7 W cm^{-2}, 5 min) (B). K+ represents the positive control. Control w/o NIR represents the negative control, while control w/ NIR represents cells solely treated with NIR light. Data represents mean ± S.D., n=5, (*p < 0.0001), ns = non-significant.

Han *et al*. previously reported that the therapeutic effect induced by poly(phosphorylcholine)-based micelles encapsulating IR780 was improved by 1.32-fold upon exposure to NIR light (808 nm, 0.6 W cm^{-2}, 10 min) [29], while the irradiation of IR-HPM improved their therapeutic capacity by 1.54-fold (808 nm, 1.7 W cm^{-2}, 5 min). In other work, the combined application of NIR light and α-Lipoic acid stabilized-based micelles loaded with Docetaxel and IR780 improved the therapeutic outcome by up to 3.26-fold [114]. In this work, a 3.35-times higher therapeutic efficacy was attained when combining NIR light and IR/DOX-HPM, which is a similar effect to that reported by Li *et al*. [114]. However, in the case of the IR/DOX-HPM formulation, a lower drug dose (1.93 *vs*. 12.5 μg mL^{-1}) and a weaker intensity (1.7 *vs*. 2.5 W cm^{-2}; 5 min) were required to achieve such effect [114]. Overall, IR/DOX-HPM are promising theragnostic devices due to their potential for being applied in cancer cell selective chemo-phototherapy and NIR imaging.

Chapter 4

Conclusion and Future Perspectives

4. Conclusion and Future Perspectives

Despite all the efforts to diminish breast cancer mortality, this disease is still a main cause of death in the world. This reality is in part owed to the sub-optimal efficacy and non-specific toxicity of the currently available treatments. To improve breast cancer treatment, researchers have been investigating novel approaches, such as light-based therapies. In this regard, NIR phototherapies mediated by IR780 display a good potential for application in cancer treatment. Moreover, this molecule can also be explored as an imaging agent, thereby being promising for cancer theragnostics. Nevertheless, IR780 presents a low water solubility and can induce acute toxicity. These problems can be surpassed by encapsulating IR780 in the core of polymeric micelles. Moreover, micelles' core can also accommodate chemotherapeutic drugs, enabling their application in cancer chemo-phototherapy. However, micelles are not intrinsically selective for the cancer cells. Therefore, the chemo-phototherapeutic effect induced by this nanoformulation can affect both the cancer and normal cells found on the tumor microenvironment, lowering their therapeutic effectiveness.

In this work, HA-*g*-PMAO was explored for the first time in the preparation of polymeric micelles encapsulating IR780 and DOX aimed for breast cancer chemo-phototherapy. The results showed that HPM prepared through the nanoprecipitation method display suitable physicochemical properties, and they are able to successfully encapsulate IR780 and the IR780-DOX combination. The encapsulation of IR780 in HPM improved its NIR absorption (at 808 nm) by about 2.2-fold, thereby enhancing the photothermal potential of IR780. Furthermore, loading IR780 in HPM also improved its cytocompatibility. In *in vitro* uptake studies, the fluorescence signals emitted by HPM were explored for cell imaging, being verified that the nanostructures were more internalized by breast cancer cells than by normal cells. These findings suggest the diagnosis potential and CD44 receptor targeting ability of these nanoformulations. Moreover, IR-HPM did not induce noticeable cytotoxic effects to breast cancer cells, while the combination of IR-HPM with NIR light led to a reduction on cells' viability up to 59 %. In turn, the combined action of IR/DOX-HPM and NIR light further decreased cells' viability to 20 %.

Overall, the HPM produced in this thesis are promising nanoplatforms for breast cancer targeted chemo-phototherapy and imaging. In the future, the inclusion of additional contrast agents in HPM core can be explored in order to develop nanoformulations for multimodal cancer imaging. Furthermore, the optimization of the large-scale production of HPM should also be pursued.

Chapter 5

References

5. References

[1] J. Ferlay, I. Soerjomataram, R. Dikshit, S. Eser, C. Mathers, M. Rebelo, D.M. Parkin, D. Forman, F. Bray, Cancer incidence and mortality worldwide: sources, methods and major patterns in GLOBOCAN 2012, International Journal of Cancer, 136 (2015) E359-386.

[2] M.J. Thun, J.O. DeLancey, M.M. Center, A. Jemal, E.M. Ward, The global burden of cancer: priorities for prevention, Carcinogenesis, 31 (2010) 100-110.

[3] P. Kumari, B. Ghosh, S. Biswas, Nanocarriers for cancer-targeted drug delivery, Journal of Drug Targeting, 24 (2016) 179-191.

[4] E. Perez-Herrero, A. Fernandez-Medarde, Advanced targeted therapies in cancer: Drug nanocarriers, the future of chemotherapy, European Journal of Pharmaceutics and Biopharmaceutics, 93 (2015) 52-79.

[5] K.-C. Chen, Y.-S. Hsieh, Y.-F. Tseng, M.-J. Shieh, J.-S. Chen, H.-S. Lai, J.-M. Lee, Pleural Photodynamic Therapy and Surgery in Lung Cancer and Thymoma Patients with Pleural Spread, PLOS ONE, 10 (2015) e0133230.

[6] A. Bucharskaya, G. Maslyakova, G. Terentyuk, A. Yakunin, Y. Avetisyan, O. Bibikova, E. Tuchina, B. Khlebtsov, N. Khlebtsov, V. Tuchin, Towards Effective Photothermal/Photodynamic Treatment Using Plasmonic Gold Nanoparticles, International Journal of Molecular Sciences, 17 (2016) 1295.

[7] X. Deng, Y. Chen, Z. Cheng, K. Deng, P.a. Ma, Z. Hou, B. Liu, S. Huang, D. Jin, J. Lin, Rational design of a comprehensive cancer therapy platform using temperature-sensitive polymer grafted hollow gold nanospheres: simultaneous chemo/photothermal/photodynamic therapy triggered by a 650 nm laser with enhanced anti-tumor efficacy, Nanoscale, 8 (2016) 6837-6850.

[8] X. Song, C. Liang, H. Gong, Q. Chen, C. Wang, Z. Liu, Photosensitizer-Conjugated Albumin-Polypyrrole Nanoparticles for Imaging-Guided In Vivo Photodynamic/Photothermal Therapy, Small, 11 (2015) 3932-3941.

[9] D. de Melo-Diogo, C. Pais-Silva, D.R. Dias, A.F. Moreira, I.J. Correia, Strategies to Improve Cancer Photothermal Therapy Mediated by Nanomaterials, Advanced Healthcare Materials, 6 (2017).

[10] N. Kosaka, M. Ogawa, P.L. Choyke, H. Kobayashi, Clinical implications of near-infrared fluorescence imaging in cancer, Future Oncology, 5 (2009) 1501-1511.

[11] D.R. Dias, A.F. Moreira, I.J. Correia, The effect of the shape of gold core-mesoporous silica shell nanoparticles on the cellular behavior and tumor spheroid penetration, Journal of Materials Chemistry B, 4 (2016) 7630-7640.

[12] D. de Melo-Diogo, C. Pais-Silva, E.C. Costa, R.O. Louro, I.J. Correia, D-α-tocopheryl polyethylene glycol 1000 succinate functionalized nanographene oxide for cancer therapy, Nanomedicine (London, England), 12 (2017) 443-456.

[13] P. Zhang, L. Zhang, Z. Qin, S. Hua, Z. Guo, C. Chu, H. Lin, Y. Zhang, W. Li, X. Zhang, X. Chen, G. Liu, Genetically Engineered Liposome-like Nanovesicles as Active Targeted Transport Platform, Advanced Materials, 30 (2018).
[14] C. Pais-Silva, D. de Melo-Diogo, I.J. Correia, IR780-loaded TPGS-TOS micelles for breast cancer photodynamic therapy, European Journal of Pharmaceutics and Biopharmaceutics, 113 (2017) 108-117.
[15] R.G. Thomas, M.J. Moon, S.P. Surendran, H.J. Park, I.K. Park, B.I. Lee, Y.Y. Jeong, MHI-148 Cyanine Dye Conjugated Chitosan Nanomicelle with NIR Light-Trigger Release Property as Cancer Targeting Theranostic Agent, Molecular Imaging and Biology, (2018).
[16] C. Zhang, S. Wang, J. Xiao, X. Tan, Y. Zhu, Y. Su, T. Cheng, C. Shi, Sentinel lymph node mapping by a near-infrared fluorescent heptamethine dye, Biomaterials, 31 (2010) 1911-1917.
[17] X. Yi, F. Wang, W. Qin, X. Yang, J. Yuan, Near-infrared fluorescent probes in cancer imaging and therapy: an emerging field, International Journal of Nanomedicine, 9 (2014) 1347-1365.
[18] U. Bazylińska, A. Lewińska, Ł. Lamch, K.A. Wilk, Polymeric nanocapsules and nanospheres for encapsulation and long sustained release of hydrophobic cyanine-type photosensitizer, Colloids and Surfaces A, 442 (2014) 42-49.
[19] Y. Yamaoka, Y. Harada, M. Sakakura, T. Minamikawa, S. Nishino, S. Maehara, S. Hamano, H. Tanaka, T. Takamatsu, Photoacoustic microscopy using ultrashort pulses with two different pulse durations, Optics Express, 22 (2014) 17063-17072.
[20] J. Kulbacka, A. Pucek, M. Kotulska, M. Dubińska-Magiera, J. Rossowska, M.-P. Rols, K.A. Wilk, Electroporation and lipid nanoparticles with cyanine IR-780 and flavonoids as efficient vectors to enhanced drug delivery in colon cancer, Bioelectrochemistry, 110 (2016) 19-31.
[21] K. Kiyose, S. Aizawa, E. Sasaki, H. Kojima, K. Hanaoka, T. Terai, Y. Urano, T. Nagano, Molecular Design Strategies for Near-Infrared Ratiometric Fluorescent Probes Based on the Unique Spectral Properties of Aminocyanines, Chemistry - A European Journal, 15 (2009) 9191-9200.
[22] F. Yan, W. Duan, Y. Li, H. Wu, Y. Zhou, M. Pan, H. Liu, X. Liu, H. Zheng, NIR-Laser-Controlled Drug Release from DOX/IR-780-Loaded Temperature-Sensitive-Liposomes for Chemo-Photothermal Synergistic Tumor Therapy, Theranostics, 6 (2016) 2337-2351.
[23] C. Yue, P. Liu, M. Zheng, P. Zhao, Y. Wang, Y. Ma, L. Cai, IR-780 dye loaded tumor targeting theranostic nanoparticles for NIR imaging and photothermal therapy, Biomaterials, 34 (2013) 6853-6861.
[24] Y. Kuang, K. Zhang, Y. Cao, X. Chen, K. Wang, M. Liu, Hydrophobic IR-780 Dye Encapsulated in cRGD-Conjugated Solid Lipid Nanoparticles for NIR Imaging-Guided Photothermal Therapy, ACS Applied Materials & Interfaces, 9 (2017) 12217-12226.
[25] C. Zhang, T. Liu, Y. Su, S. Luo, Y. Zhu, X. Tan, S. Fan, L. Zhang, Y. Zhou, T. Cheng, C. Shi, A near-infrared fluorescent heptamethine indocyanine dye with preferential tumor accumulation for in vivo imaging, Biomaterials, 31 (2010) 6612-6617.

[26] X. Yi, F. Yan, F. Wang, W. Qin, G. Wu, X. Yang, C. Shao, L.W. Chung, J. Yuan, IR-780 dye for near-infrared fluorescence imaging in prostate cancer, Medical Science Monitor, 21 (2015) 511-517.
[27] X. Yi, J. Zhang, F. Yan, Z. Lu, J. Huang, C. Pan, J. Yuan, W. Zheng, K. Zhang, D. Wei, W. He, J. Yuan, Synthesis of IR-780 dye-conjugated abiraterone for prostate cancer imaging and therapy, International Journal of Oncology, 49 (2016) 1911-1920.
[28] Y. Chen, Z. Li, H. Wang, Y. Wang, H. Han, Q. Jin, J. Ji, IR-780 Loaded Phospholipid Mimicking Homopolymeric Micelles for Near-IR Imaging and Photothermal Therapy of Pancreatic Cancer, ACS Applied Materials & Interfaces, 8 (2016) 6852-6858.
[29] H. Han, S. Zhang, Y. Wang, T. Chen, Q. Jin, Y. Chen, Z. Li, J. Ji, Biomimetic drug nanocarriers prepared by miniemulsion polymerization for near-infrared imaging and photothermal therapy, Polymer, 82 (2016) 255-261.
[30] H. Han, J. Wang, T. Chen, L. Yin, Q. Jin, J. Ji, Enzyme-sensitive gemcitabine conjugated albumin nanoparticles as a versatile theranostic nanoplatform for pancreatic cancer treatment, Journal of Colloid and Interface Science, 507 (2017) 217-224.
[31] C.-S. Yeh, C.-H. Su, W.-Y. Ho, C.-C. Huang, J.-C. Chang, Y.-H. Chien, S.-T. Hung, M.-C. Liau, H.-Y. Ho, Tumor targeting and MR imaging with lipophilic cyanine-mediated near-infrared responsive porous Gd silicate nanoparticles, Biomaterials, 34 (2013) 5677-5688.
[32] H. Li, K. Wang, X. Yang, Y. Zhou, Q. Ping, D. Oupicky, M. Sun, Dual-function nanostructured lipid carriers to deliver IR780 for breast cancer treatment: Anti-metastatic and photothermal anti-tumor therapy, Acta Biomaterialia, 53 (2017) 399-413.
[33] S. Uthaman, A.P. Mathew, H.J. Park, B.-I. Lee, H.-S. Kim, K.M. Huh, I.-K. Park, IR 780-loaded hyaluronic acid micelles for enhanced tumor-targeted photothermal therapy, Carbohydrate Polymers, 181 (2018) 1-9.
[34] A. Yuan, X. Qiu, X. Tang, W. Liu, J. Wu, Y. Hu, Self-assembled PEG-IR-780-C13 micelle as a targeting, safe and highly-effective photothermal agent for in vivo imaging and cancer therapy, Biomaterials, 51 (2015) 184-193.
[35] C. Jiang, H. Cheng, A. Yuan, X. Tang, J. Wu, Y. Hu, Hydrophobic IR780 encapsulated in biodegradable human serum albumin nanoparticles for photothermal and photodynamic therapy, Acta Biomaterialia, 14 (2015) 61-69.
[36] C. Zhao, Y. Tong, X. Li, L. Shao, L. Chen, J. Lu, X. Deng, X. Wang, Y. Wu, Photosensitive Nanoparticles Combining Vascular-Independent Intratumor Distribution and On-Demand Oxygen-Depot Delivery for Enhanced Cancer Photodynamic Therapy, Small, (2018).
[37] C.-L. Peng, Y.-H. Shih, P.-C. Lee, T.M.-H. Hsieh, T.-Y. Luo, M.-J. Shieh, Multimodal image-guided photothermal therapy mediated by 188Re-labeled micelles containing a cyanine-type photosensitizer, ACS Nano, 5 (2011) 5594-5607.
[38] B. He, H.-y. Hu, T. Tan, H. Wang, K.-x. Sun, Y.-p. Li, Z.-w. Zhang, IR-780-loaded polymeric micelles enhance the efficacy of photothermal therapy in treating breast cancer lymphatic metastasis in mice, Acta Pharmacologica Sinica, 39 (2017) 132-139.

[39] C. Yue, Y. Yang, J. Song, G. Alfranca, C. Zhang, Q. Zhang, T. Yin, F. Pan, J.M. de la Fuente, D. Cui, Mitochondria-targeting near-infrared light-triggered thermosensitive liposomes for localized photothermal and photodynamic ablation of tumors combined with chemotherapy, Nanoscale, 9 (2017) 11103-11118.
[40] T. Lin, A. Yuan, X. Zhao, H. Lian, J. Zhuang, W. Chen, Q. Zhang, G. Liu, S. Zhang, W. Chen, W. Cao, C. Zhang, J. Wu, Y. Hu, H. Guo, Self-assembled tumor-targeting hyaluronic acid nanoparticles for photothermal ablation in orthotopic bladder cancer, Acta Biomaterialia, 53 (2017) 427-438.
[41] K. Wang, Y. Zhang, J. Wang, A. Yuan, M. Sun, J. Wu, Y. Hu, Self-assembled IR780-loaded transferrin nanoparticles as an imaging, targeting and PDT/PTT agent for cancer therapy, Scientific Reports, 6 (2016) 27421.
[42] Z. Li, H. Wang, Y. Chen, Y. Wang, H. Li, H. Han, T. Chen, Q. Jin, J. Ji, pH- and NIR Light-Responsive Polymeric Prodrug Micelles for Hyperthermia-Assisted Site-Specific Chemotherapy to Reverse Drug Resistance in Cancer Treatment, Small, 12 (2016) 2731-2740.
[43] S.K. Hobbs, W.L. Monsky, F. Yuan, W.G. Roberts, L. Griffith, V.P. Torchilin, R.K. Jain, Regulation of transport pathways in tumor vessels: role of tumor type and microenvironment, Proceedings of the National Academy Sciences of the U S A, 95 (1998) 4607-4612.
[44] E. Blanco, H. Shen, M. Ferrari, Principles of nanoparticle design for overcoming biological barriers to drug delivery, Nature Biotechnology, 33 (2015) 941-951.
[45] S.P. Egusquiaguirre, M. Igartua, R.M. Hernandez, J.L. Pedraz, Nanoparticle delivery systems for cancer therapy: advances in clinical and preclinical research, Clinical & Translational Oncology, 14 (2012) 83-93.
[46] H. Soo Choi, W. Liu, P. Misra, E. Tanaka, J.P. Zimmer, B. Itty Ipe, M.G. Bawendi, J.V. Frangioni, Renal clearance of quantum dots, Nature Biotechnology, 25 (2007) 1165-1170.
[47] M.J. Ernsting, M. Murakami, A. Roy, S.D. Li, Factors controlling the pharmacokinetics, biodistribution and intratumoral penetration of nanoparticles, Journal of Controlled Release, 172 (2013) 782-794.
[48] G. Sonavane, K. Tomoda, K. Makino, Biodistribution of colloidal gold nanoparticles after intravenous administration: effect of particle size, Colloids and Surfaces B, 66 (2008) 274-280.
[49] K. Huang, H. Ma, J. Liu, S. Huo, A. Kumar, T. Wei, X. Zhang, S. Jin, Y. Gan, P.C. Wang, S. He, X. Zhang, X.-J. Liang, Size-Dependent Localization and Penetration of Ultrasmall Gold Nanoparticles in Cancer Cells, Multicellular Spheroids, and Tumors in Vivo, ACS Nano, 6 (2012) 4483-4493.
[50] E.C. Cho, L. Au, Q. Zhang, Y. Xia, The effects of size, shape, and surface functional group of gold nanostructures on their adsorption and internalization by cells, Small, 6 (2010) 517-522.
[51] Z. Popovic, W. Liu, V.P. Chauhan, J. Lee, C. Wong, A.B. Greytak, N. Insin, D.G. Nocera, D. Fukumura, R.K. Jain, M.G. Bawendi, A nanoparticle size series for in vivo fluorescence imaging, Angewandte Chemie International Edition, 49 (2010) 8649-8652.

[52] E. Bastien, R. Schneider, S. Hackbarth, D. Dumas, J. Jasniewski, B. Röder, L. Bezdetnaya, H.-P. Lassalle, PAMAM G4.5-chlorin e6 dendrimeric nanoparticles for enhanced photodynamic effects, Photochemical & Photobiological Sciences, 14 (2015) 2203-2212.
[53] H.A. Isakau, M.V. Parkhats, V.N. Knyukshto, B.M. Dzhagarov, E.P. Petrov, P.T. Petrov, Toward understanding the high PDT efficacy of chlorin e6–polyvinylpyrrolidone formulations: Photophysical and molecular aspects of photosensitizer–polymer interaction in vitro, Journal of Photochemistry and Photobiology B, 92 (2008) 165-174.
[54] A. Kamkaew, S.H. Lim, H.B. Lee, L.V. Kiew, L.Y. Chung, K. Burgess, BODIPY dyes in photodynamic therapy, Chemical Society Reviews, 42 (2013) 77-88.
[55] A.P. Losev, I.N. Nichiporovich, I.N. Zhuravkin, E.A. Zhavrid, "Energetics of chlorins: a potent photosensitizer of PDT", Proc. SPIE 2675, Optical Methods for Tumor Treatment and Detection: Mechanisms and Techniques in Photodynamic Therapy V., (1996).
[56] M.R. Hamblin, M.P. Bamberg, J.L. Miller, T. Hasan, Cationic photoimmunoconjugates between monoclonal antibodies and hematoporphyrin: selective photodestruction of ovarian cancer cells, Applied Optics, 37 (1998) 7184-7192.
[57] X. Peng, D.R. Draney, W.M. Volcheck, G.R. Bashford, D.T. Lamb, D.L. Grone, Y. Zhang, C.M. Johnson, "Phthalocyanine dye as an extremely photostable and highly fluorescent near-infrared labeling reagent", Proc. SPIE 6097, Optical Molecular Probes for Biomedical Applications, 60970E., (2006).
[58] S. Kishimoto, M. Bernardo, K. Saito, S. Koyasu, J.B. Mitchell, P.L. Choyke, M.C. Krishna, Evaluation of oxygen dependence on in vitro and in vivo cytotoxicity of photoimmunotherapy using IR-700–antibody conjugates, Free Radical Biology and Medicine, 85 (2015) 24-32.
[59] X. Peng, H. Chen, D.R. Draney, W. Volcheck, A. Schutz-Geschwender, D.M. Olive, A nonfluorescent, broad-range quencher dye for Förster resonance energy transfer assays, Analytical Biochemistry, 388 (2009) 220-228.
[60] B. Simard, B. Tomanek, F.C. van Veggel, A. Abulrob, Optimal dye-quencher pairs for the design of an “activatable” nanoprobe for optical imaging, Photochemical & Photobiological Sciences, 12 (2013) 1824-1829.
[61] B. Simard, G.G. Mironov, B. Tomanek, F.C. Veggel, A. Abulrob, Site-specific conjugation of the quencher on peptide's N-terminal for the synthesis of a targeted non-spreading activatable optical probe, Journal of Peptide Science, 22 (2016) 415-420.
[62] A. Shrivastava, H. Ding, S. Kothandaraman, S.-H. Wang, L. Gong, M. Williams, K. Milum, S. Zhang, M.F. Tweedle, A high-affinity near-infrared fluorescent probe to target bombesin receptors, Molecular Imaging and Biology, 16 (2014) 661-669.
[63] D.S. Conceição, D.P. Ferreira, L.F.V. Ferreira, Photochemistry and cytotoxicity evaluation of heptamethinecyanine Near Infrared (NIR) dyes, International Journal of Molecular Sciences, 14 (2013) 18557-18571.
[64] Y. Cheng, H. Cheng, C. Jiang, X. Qiu, K. Wang, W. Huan, A. Yuan, J. Wu, Y. Hu, Perfluorocarbon nanoparticles enhance reactive oxygen levels and tumour growth inhibition in photodynamic therapy, Nature Communications, 6 (2015) 8785.

[65] K. Licha, B. Riefke, V. Ntziachristos, A. Becker, B. Chance, W. Semmler, Hydrophilic Cyanine Dyes as Contrast Agents for Near-infrared Tumor Imaging: Synthesis, Photophysical Properties and Spectroscopic In vivo Characterization, Photochemistry and Photobiology, 72 (2000) 392-398.
[66] N.S. James, Y. Chen, P. Joshi, T.Y. Ohulchanskyy, M. Ethirajan, M. Henary, L. Strekowsk, R.K. Pandey, Evaluation of polymethine dyes as potential probes for near infrared fluorescence imaging of tumors: part-1, Theranostics, 3 (2013) 692-702.
[67] X. Yang, C. Shi, R. Tong, W. Qian, H.E. Zhau, R. Wang, G. Zhu, J. Cheng, V.W. Yang, T. Cheng, Near IR heptamethine cyanine dye–mediated cancer imaging, Clinical Cancer Research, 16 (2010) 2833-2844.
[68] G. Sahay, D.Y. Alakhova, A.V. Kabanov, Endocytosis of nanomedicines, Journal of Controlled Release, 145 (2010) 182-195.
[69] R.K. Jain, T. Stylianopoulos, Delivering nanomedicine to solid tumors, Nature Reviews Clinical Oncology, 7 (2010) 653-664.
[70] B.-S. Kim, C.-S. Kim, K.-M. Lee, The intracellular uptake ability of chitosan-coated Poly (D,L-lactide-co-glycolide) nanoparticles, Archives of Pharmacal Research, 31 (2008) 1050-1054.
[71] M. Roser, D. Fischer, T. Kissel, Surface-modified biodegradable albumin nano- and microspheres. II: effect of surface charges on in vitro phagocytosis and biodistribution in rats, European Journal of Pharmaceutics and Biopharmaceutics, 46 (1998) 255-263.
[72] A.S. Zahr, C.A. Davis, M.V. Pishko, Macrophage uptake of core-shell nanoparticles surface modified with poly(ethylene glycol), Langmuir, 22 (2006) 8178-8185.
[73] C. Chouly, D. Pouliquen, I. Lucet, J.J. Jeune, P. Jallet, Development of superparamagnetic nanoparticles for MRI: effect of particle size, charge and surface nature on biodistribution, Journal of Microencapsulation, 13 (1996) 245-255.
[74] A. Villanueva, M. Cañete, A.G. Roca, M. Calero, S. Veintemillas-Verdaguer, C.J. Serna, M.d.P. Morales, R. Miranda, The influence of surface functionalization on the enhanced internalization of magnetic nanoparticles in cancer cells, Nanotechnology, 20 (2009) 115103.
[75] A. Lesniak, F. Fenaroli, M.P. Monopoli, C. Aberg, K.A. Dawson, A. Salvati, Effects of the presence or absence of a protein corona on silica nanoparticle uptake and impact on cells, ACS Nano, 6 (2012) 5845-5857.
[76] K. Saha, M. Rahimi, M. Yazdani, S.T. Kim, D.F. Moyano, S. Hou, R. Das, R. Mout, F. Rezaee, M. Mahmoudi, V.M. Rotello, Regulation of Macrophage Recognition through the Interplay of Nanoparticle Surface Functionality and Protein Corona, ACS Nano, 10 (2016) 4421-4430.
[77] W. Yang, L. Zhang, S. Wang, A.D. White, S. Jiang, Functionalizable and ultra stable nanoparticles coated with zwitterionic poly(carboxybetaine) in undiluted blood serum, Biomaterials, 30 (2009) 5617-5621.
[78] C. von Roemeling, W. Jiang, C.K. Chan, I.L. Weissman, B.Y. Kim, Breaking Down the Barriers to Precision Cancer Nanomedicine, Trends in Biotechnology, 35 (2017) 159-171.
[79] J.L. Perry, K.G. Reuter, M.P. Kai, K.P. Herlihy, S.W. Jones, J.C. Luft, M. Napier, J.E. Bear, J.M. DeSimone, PEGylated PRINT nanoparticles: the impact of PEG density on protein binding,

macrophage association, biodistribution, and pharmacokinetics, Nano Letters, 12 (2012) 5304-5310.
[80] Y. Zhai, Y. Zhao, J. Lei, Z. Su, G. Ma, Enhanced circulation half-life of site-specific PEGylated rhG-CSF: optimization of PEG molecular weight, Journal of Biotechnology, 142 (2009) 259-266.
[81] X. Liu, H. Tao, K. Yang, S. Zhang, S.-T. Lee, Z. Liu, Optimization of surface chemistry on single-walled carbon nanotubes for in vivo photothermal ablation of tumors, Biomaterials, 32 (2011) 144-151.
[82] F. Guo, M. Yu, J. Wang, F. Tan, N. Li, Smart IR780 Theranostic Nanocarrier for Tumor-Specific Therapy: Hyperthermia-Mediated Bubble-Generating and Folate-Targeted Liposomes, ACS Applied Materials & Interfaces, 7 (2015) 20556-20567.
[83] J. Choi, E. Rustique, M. Henry, M. Guidetti, V. Josserand, L. Sancey, J. Boutet, J.L. Coll, Targeting tumors with cyclic RGD-conjugated lipid nanoparticles loaded with an IR780 NIR dye: In vitro and in vivo evaluation, International Journal of Pharmaceutics, 532 (2017) 677-685.
[84] W. Tao, X. Zeng, J. Wu, X. Zhu, X. Yu, X. Zhang, J. Zhang, G. Liu, L. Mei, Polydopamine-Based Surface Modification of Novel Nanoparticle-Aptamer Bioconjugates for In Vivo Breast Cancer Targeting and Enhanced Therapeutic Effects, Theranostics, 6 (2016) 470-484.
[85] Y.-H. Shih, T.-Y. Luo, P.-F. Chiang, C.-J. Yao, W.-J. Lin, C.-L. Peng, M.-J. Shieh, EGFR-targeted micelles containing near-infrared dye for enhanced photothermal therapy in colorectal cancer, Journal of Controlled Release, 258 (2017) 196-207.
[86] D.R. Elias, A. Poloukhtine, V. Popik, A. Tsourkas, Effect of ligand density, receptor density, and nanoparticle size on cell targeting, Nanomedicine (N. Y., NY, U. S.), 9 (2013) 194-201.
[87] M. Dunne, J. Zheng, J. Rosenblat, D.A. Jaffray, C. Allen, APN/CD13-targeting as a strategy to alter the tumor accumulation of liposomes, Journal of Controlled Release, 154 (2011) 298-305.
[88] B.-X. Zhao, Y. Zhao, Y. Huang, L.-M. Luo, P. Song, X. Wang, S. Chen, K.-F. Yu, X. Zhang, Q. Zhang, The efficiency of tumor-specific pH-responsive peptide-modified polymeric micelles containing paclitaxel, Biomaterials, 33 (2012) 2508-2520.
[89] Q. Dai, C. Walkey, W.C. Chan, Polyethylene glycol backfilling mitigates the negative impact of the protein corona on nanoparticle cell targeting, Angewandte Chemie (International Edition in English), 53 (2014) 5093-5096.
[90] K.F. Chu, D.E. Dupuy, Thermal ablation of tumours: biological mechanisms and advances in therapy, Nature Reviews Cancer, 14 (2014) 199-208.
[91] A.P. Castano, T.N. Demidova, M.R. Hamblin, Mechanisms in photodynamic therapy: part one—photosensitizers, photochemistry and cellular localization, Photodiagnosis and Photodynamic Therapy, 1 (2004) 279-293.
[92] S. Luo, E. Zhang, Y. Su, T. Cheng, C. Shi, A review of NIR dyes in cancer targeting and imaging, Biomaterials, 32 (2011) 7127-7138.

[93] Y. Zhan, X. Cao, X. Cao, Y. Li, J. Tian, J. Liang, X. Chen, Silica Cross-Linked Micellar Core-Shell Nanoparticles Encapsulating IR-780 with Strong Bright and Good Biocompatibility for Optical Imaging *In Vivo*, Journal of Biomedical Nanotechnology, 13 (2017) 144-154.
[94] S. Li, S. Zhou, Y. Li, X. Li, J. Zhu, L. Fan, S. Yang, Exceptionally High Payload of the IR780 Iodide on Folic Acid-Functionalized Graphene Quantum Dots for Targeted Photothermal Therapy, ACS Applied Materials & Interfaces, 9 (2017) 22332-22341.
[95] Y. Zhang, L. He, J. Wu, K. Wang, J. Wang, W. Dai, A. Yuan, J. Wu, Y. Hu, Switchable PDT for reducing skin photosensitization by a NIR dye inducing self-assembled and photo-disassembled nanoparticles, Biomaterials, 107 (2016) 23-32.
[96] H. Cao, L. Zou, B. He, L. Zeng, Y. Huang, H. Yu, P. Zhang, Q. Yin, Z. Zhang, Y. Li, Albumin Biomimetic Nanocorona Improves Tumor Targeting and Penetration for Synergistic Therapy of Metastatic Breast Cancer, Advanced Functional Materials, 27 (2017) 1605679-n/a.
[97] T.H. Tran, H.T. Nguyen, T.T. Phuong Tran, S.K. Ku, J.-H. Jeong, H.-G. Choi, C.S. Yong, J.O. Kim, Combined photothermal and photodynamic therapy by hyaluronic acid-decorated polypyrrole nanoparticles, Nanomedicine, 12 (2017).
[98] Y. Hao, B. Zhang, C. Zheng, R. Ji, X. Ren, F. Guo, S. Sun, J. Shi, H. Zhang, Z. Zhang, L. Wang, Y. Zhang, The tumor-targeting core–shell structured DTX-loaded PLGA@Au nanoparticles for chemo-photothermal therapy and X-ray imaging, Journal of Controlled Release, 220 (2015) 545-555.
[99] W. He, X. Hu, W. Jiang, R. Liu, D. Zhang, J. Zhang, Z. Li, Y. Luan, Rational Design of a New Self-Codelivery System from Redox-Sensitive Camptothecin–Cytarabine Conjugate Assembly for Effectively Synergistic Anticancer Therapy, Advanced Healthcare Materials, 6 (2017) 1700829.
[100] J. Yoo, N. Sanoj Rejinold, D. Lee, S. Jon, Y.-C. Kim, Protease-activatable cell-penetrating peptide possessing ROS-triggered phase transition for enhanced cancer therapy, Journal of Controlled Release, 264 (2017) 89-101.
[101] V.M. Platt, F.C. Szoka, Jr., Anticancer therapeutics: targeting macromolecules and nanocarriers to hyaluronan or CD44, a hyaluronan receptor, Molecular Pharmaceutics, 5 (2008) 474-486.
[102] H.J. Cho, H.Y. Yoon, H. Koo, S.H. Ko, J.S. Shim, J.H. Lee, K. Kim, I.C. Kwon, D.D. Kim, Self-assembled nanoparticles based on hyaluronic acid-ceramide (HA-CE) and Pluronic(R) for tumor-targeted delivery of docetaxel, Biomaterials, 32 (2011) 7181-7190.
[103] L. Qiu, Z. Li, M. Qiao, M. Long, M. Wang, X. Zhang, C. Tian, D. Chen, Self-assembled pH-responsive hyaluronic acid-g-poly((L)-histidine) copolymer micelles for targeted intracellular delivery of doxorubicin, Acta Biomaterialia, 10 (2014) 2024-2035.
[104] C. Yang, Y. He, H. Zhang, Y. Liu, W. Wang, Y. Du, F. Gao, Selective killing of breast cancer cells expressing activated CD44 using CD44 ligand-coated nanoparticles in vitro and in vivo, Oncotarget, 6 (2015) 15283-15296.

[105] Y. Miyatake, A.L.A. Oliveira, M.A. Jarboui, S. Ota, U. Tomaru, T. Teshima, W.W. Hall, M. Kasahara, Protective Roles of Epithelial Cells in the Survival of Adult T-Cell Leukemia/Lymphoma Cells, The American Journal of Pathology, 182 (2013) 1832-1842.
[106] C.G. Alves, R. Lima-Sousa, D. de Melo-Diogo, R.O. Louro, I.J. Correia, IR780 based nanomaterials for cancer imaging and photothermal, photodynamic and combinatorial therapies, International Journal of Pharmaceutics, 542 (2018) 164-175.
[107] J. Qi, P. Yao, F. He, C. Yu, C. Huang, Nanoparticles with dextran/chitosan shell and BSA/chitosan core—Doxorubicin loading and delivery, International Journal of Pharmaceutics, 393 (2010) 177-185.
[108] J. Li, M. Huo, J. Wang, J. Zhou, J.M. Mohammad, Y. Zhang, Q. Zhu, A.Y. Waddad, Q. Zhang, Redox-sensitive micelles self-assembled from amphiphilic hyaluronic acid-deoxycholic acid conjugates for targeted intracellular delivery of paclitaxel, Biomaterials, 33 (2012) 2310-2320.
[109] J. Huang, H. Zhang, Y. Yu, Y. Chen, D. Wang, G. Zhang, G. Zhou, J. Liu, Z. Sun, D. Sun, Y. Lu, Y. Zhong, Biodegradable self-assembled nanoparticles of poly (D,L-lactide-co-glycolide)/hyaluronic acid block copolymers for target delivery of docetaxel to breast cancer, Biomaterials, 35 (2014) 550-566.
[110] Y. Li, M. Kroger, W.K. Liu, Shape effect in cellular uptake of PEGylated nanoparticles: comparison between sphere, rod, cube and disk, Nanoscale, 7 (2015) 16631-16646.
[111] S. Cheon Lee, C. Kim, I. Chan Kwon, H. Chung, S. Young Jeong, Polymeric micelles of poly(2-ethyl-2-oxazoline)-block-poly(epsilon-caprolactone) copolymer as a carrier for paclitaxel, Journal of Controlled Release, 89 (2003) 437-446.
[112] L. Yan, H. Wang, A. Zhang, C. Zhao, Y. Chen, X. Li, Bright and stable near-infrared Pluronic-silica nanoparticles as contrast agents for in vivo optical imaging, Journal of Materials Chemistry B, 4 (2016) 5560-5566.
[113] T. Nagy-Simon, M. Potara, A.M. Craciun, E. Licarete, S. Astilean, IR780-dye loaded gold nanoparticles as new near infrared activatable nanotheranostic agents for simultaneous photodynamic and photothermal therapy and intracellular tracking by surface enhanced resonant Raman scattering imaging, Journal of Colloid and Interface Science, 517 (2018) 239-250.
[114] W. Li, J. Peng, Q. Yang, L. Chen, L. Zhang, X. Chen, Z. Qian, α-Lipoic acid stabilized DTX/IR780 micelles for photoacoustic/fluorescence imaging guided photothermal therapy/chemotherapy of breast cancer, Biomaterials Science, 6 (2018) 1201-1216.
[115] W. Takehiko, C. Suwabun, I. Naoto, I. Yoshiaki, T. Kchi, Synthesis and Properties of Hyaluronic Acid Conjugated Nucleic Acid Analogs—1: Synthesis of Deacetylhyaluronan and Introduction of Nucleic Acid Bases, Journal of Bioactive and Compatible Polymers, 9 (1994) 429-447.
[116] S.M. Henry, M.E.H. El-Sayed, C.M. Pirie, A.S. Hoffman, P.S. Stayton, pH-Responsive Poly(styrene-alt-maleic anhydride) Alkylamide Copolymers for Intracellular Drug Delivery, Biomacromolecules, 7 (2006) 2407-2414.

[117] J. Qiu, R. Cheng, J. Zhang, H. Sun, C. Deng, F. Meng, Z. Zhong, Glutathione-Sensitive Hyaluronic Acid-Mercaptopurine Prodrug Linked via Carbonyl Vinyl Sulfide: A Robust and CD44-Targeted Nanomedicine for Leukemia, Biomacromolecules, 18 (2017) 3207-3214.

Chapter 6

Appendix

6. Appendix

6.1. Deacetylation of Hyaluronic acid

Deacetylation of Hyaluronic acid (HA) was performed according to a method described elsewhere [115]. Briefly, Hyaluronic acid (0.25 g) was dissolved in 12.5 mL of NaOH solution 13.7 N. This solution was left to react for 2 h, at 60 °C, under stirring. Then, the solutions' pH was adjusted to 7 using HCl. Finally, the solution was dialysed against water (using 3.5 KDa molecular weight cut-off dialysis membrane) and freeze-dried, yielding deacetylated Hyaluronic acid (dHA).

Fourier Transform Infrared Spectroscopy (FTIR) analysis was performed to confirm the production of dHA (Figure 14). Prior to the deacetylation, a peak at 1738 cm^{-1} (C=O) was observed in HA spectrum, belonging to the HA ketone groups. After the alkaline hydrolysis, the intensity of this peak decreased, thereby confirming the successful deacetylation of Hyaluronic acid (Figure 14).

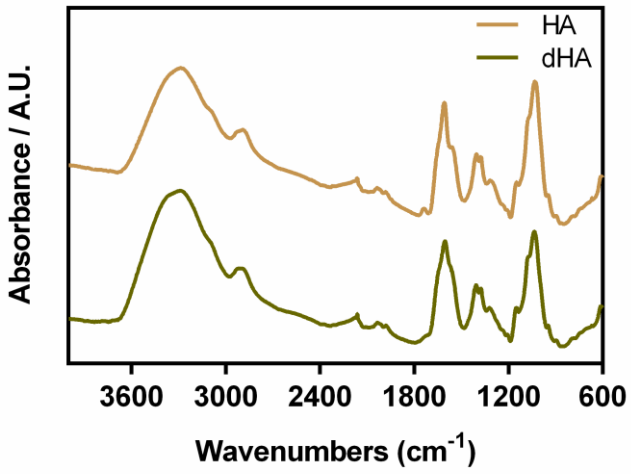

Figure 14. FTIR spectra of HA and dHA.

6.2. Hydrolysis of PMAO

The hydrolysis of poly(maleic anhydride-*alt*-1-octadecene) (PMAO) anhydride rings was performed as described elsewhere [116]. Briefly, PMAO (0.2 g) was dissolved in 4 mL of NaOH 2 N and stirred at room temperature for 5 h. Afterwards, the solution was neutralized using HCl. Finally, the solution was dialysed against water (14 KDa molecular weight cut-off dialysis membrane) and freeze-dried, yielding PMAO with its rings open (oPMAO).

The FTIR spectrum of PMAO displayed peaks at 1857 and 1777 cm^{-1} (C=O stretch of anhydrides), which disappeared after the hydrolysis (Figure 15). Moreover, the spectrum of oPMAO presented additional peaks at 1706 and 1559 cm^{-1} (C=O stretches of carboxylic acids), thereby proving its successful preparation (Figure 15).

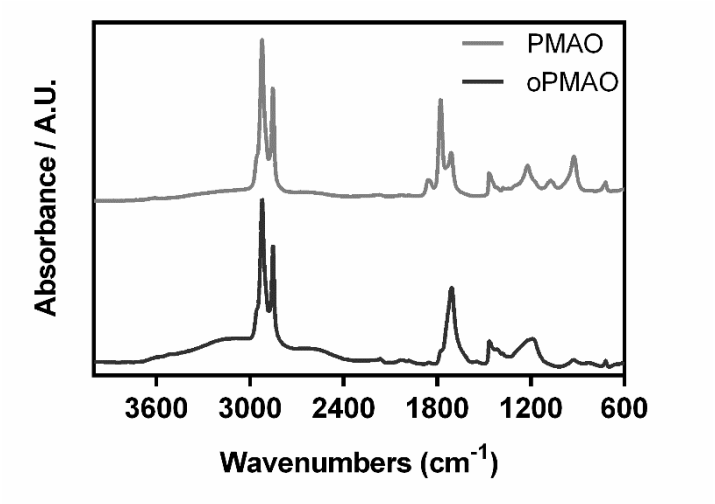

Figure 15. FTIR spectra of PMAO and oPMAO.

6.3. Synthesis of HA-*g*-PMAO

HA grafted PMAO (HA-*g*-PMAO) was produced by adapting a protocol described in the literature [117]. First oPMAO (0.05 g) was activated with EDC and NHS (0.5 equivalents of each compound) in 25 mL of DMSO for 1 h. Then, 25 mL of water containing dHA (0.05 g) were added and the reaction was carried out for 6.5 h (room temperature). Afterwards, the solution was dialysed against water (14 KDa molecular weight cut-off dialysis membrane) and freeze-dried, yielding HA-*g*-PMAO.

The FTIR spectra of HA-*g*-PMAO and oPMAO (Figure 16) presented peaks at 2921 and 2851 cm^{-1} (C-H stretches), belonging to the alkyl chain of PMAO. The spectra of dHA and HA-*g*-PMAO both present a peak at 1042 cm^{-1} (C-O stretch of primary alcohol) (Figure 16). Furthermore, the peak at 1640 cm^{-1} (C=O of secondary amide) displayed in the spectrum of HA-*g*-PMAO further corroborates the conjugation of dHA with oPMAO (Figure 16).

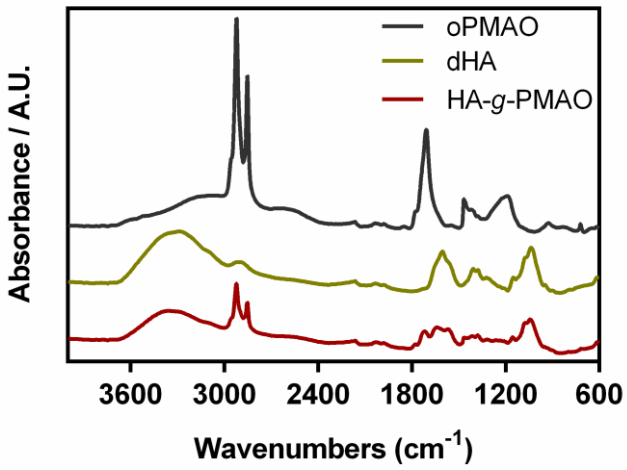

Figure 16. FTIR spectra of oPMAO, dHA and HA-*g*-PMAO.